

---

# **SCIENTIFIC NOTEBOOK 1005E**

---

**Infiltration and Unsaturated Zone Confirmatory Analyses**

*by*

**Stuart A. Stothoff**

**Southwest Research Institute  
Center for Nuclear Waste Regulatory Analyses  
San Antonio, Texas**

**June 30, 2010**

## Initial Entries

Scientific NoteBook: #1005E

Title: Infiltration and Unsaturated Zone Confirmatory Analyses

Issued to: S. A. Stothoff

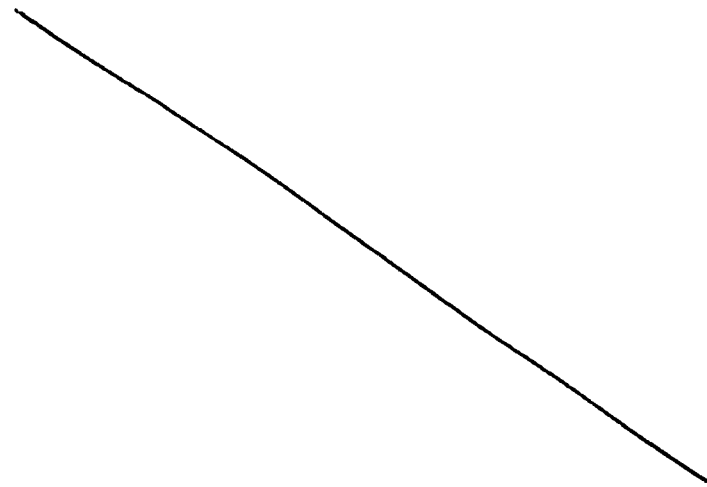


Issue Date: August 31, 2009

This computerized Scientific NoteBook is intended to address the criteria of CNWRA QAP-001.

This scientific notebook is intended to document confirmatory analyses for the Safety Evaluation Review of the Department of Energy (DOE) Safety Analysis Report and supporting documents describing the suitability of the Yucca Mountain site for emplacement of high-level radioactive waste. The objective of these analyses is to examine particular assumptions and calculations that DOE provided related to infiltration and percolation within the unsaturated zone under ambient conditions. The analyses will rely on independent numerical calculations.

The notebook consists of several chapters. Each chapter of the notebook describes the objectives and approaches for a separate analysis. The last two chapters provide supplemental information and analyses that informed the Safety Evaluation Review but were not directly cited.



RL 7/6/2010

**Contents**

<b>Initial Entries</b>	<b>ii</b>
<b>List of Figures</b>	<b>xiii</b>
<b>List of Tables</b>	<b>xiv</b>
<b>1 Aspects of infiltration</b>	<b>1-1</b>
08/28/09 Analysis of precipitation duration . . . . .	1-1
<b>2 Infiltration, percolation, and seepage</b>	<b>2-1</b>
10/26/09 Seepage and flow focusing . . . . .	2-1
11/06/09 Seepage and flow focusing . . . . .	2-5
06/25/10 Supplemental information on seepage . . . . .	2-7
<b>3 Safety Evaluation Review calculations</b>	<b>3-1</b>
04/20/10 Decadal climate variability analysis from SER Section 2.2.1.3.6.2 . . . . .	3-1
04/21/10 Episodic flow analysis from SER Section 2.2.1.3.6.2 . . . . .	3-2
04/22/10 Temporal variability from SER Section 2.2.1.3.5.3.2.2 . . . . .	3-4
04/22/10 Uncertain soil depth from SER Section 2.2.1.3.5.3.3 . . . . .	3-5
<b>4 Safety Evaluation Review supplemental notes</b>	<b>4-1</b>
06/15/10 TSPA realization dose histories . . . . .	4-1
06/15/10 Transport and release supplemental simulations . . . . .	4-8
06/16/10 Direct seepage effects on diffusive releases . . . . .	4-15

06/18/10	Direct seepage effects from parameters . . . . .	4-19
06/21/10	More direct seepage effects from parameters . . . . .	4-23
06/22/10	Return to seepage effects on diffusive releases . . . . .	4-33
06/23/10	More seepage effects on releases . . . . .	4-44
06/24/10	Seepage effects on transient releases . . . . .	4-56
06/26/10	Model effects on transient partitioning . . . . .	4-83
<b>5</b>	<b>Site-scale unsaturated zone flow model visualization</b>	<b>5-1</b>
06/28/10	Supplemental information on percolation . . . . .	5-1
06/29/10	Infiltration and percolation redistribution . . . . .	5-1
06/30/10	Percolation and saturation slices . . . . .	5-25
	<b>Code listing appendix for infiltration, percolation, and seepage</b>	<b>A-1</b>
04/21/10	test_DOE_seepratecurve.m . . . . .	A-1
04/23/10	test_massif_precip.m . . . . .	A-5
	<b>Final QA Information</b>	<b>i</b>

## List of Figures

2-1	DOE abstraction for seepage in TSPA. Tabulated values indicated with circles and an independent functional form indicated by curves. Parameter values used in TSPA are indicated. . . . .	2-2
2-2	Cumulative distribution function for areal-average seepage under nominal conditions.	2-4
2-3	TSPA results from the seepageDLL routine for the 10th percentile infiltration scenario of the glacial transition climate for the CDSP waste packages. . . . .	2-6
2-4	Cumulative distribution curves for the 10th percentile infiltration scenario of the glacial transition climate, comparing drift-scale and repository-average distributions.	2-8
2-5	The fitted relationship (red) between $1/\alpha$ and $K_f/Q_p$ estimated from simulations (black). . . . .	2-10
2-6	The nominal flow focusing factor representation compared with lognormal distributions having the same mean. . . . .	2-11
3-1	Simulated precipitation sequences using SNL parameters for present-day climate and 10,000 realizations. (a) Monthly precipitation sequences, (b) cumulative frequency, and (c) correlation between annual and seasonal precipitation. . . . .	3-6
3-2	Simulated precipitation sequences using SNL parameters for monsoon climate and 10,000 realizations. (a) Monthly precipitation sequences, (b) cumulative frequency, and (c) correlation between annual and seasonal precipitation. . . . .	3-7
3-3	Simulated precipitation sequences using SNL parameters for glacial-transition climate and 10,000 realizations. (a) Monthly precipitation sequences, (b) cumulative frequency, and (c) correlation between annual and seasonal precipitation. . . . .	3-8
4-1	Nominal scenario realizations and expected values from TSPA LA simulations, partitioned according to infiltration scenario. Expected peak doses and maximum expected doses are indicated. . . . .	4-2
4-2	Igneous scenario realizations and expected values from TSPA LA simulations, partitioned according to infiltration scenario. Expected peak doses and maximum expected doses are indicated. . . . .	4-3

4-3	Seismic scenario realizations and expected values from TSPA LA simulations, partitioned according to infiltration scenario. Expected peak doses and maximum expected doses are indicated. . . . .	4-4
4-4	Nominal scenario realizations and expected values from TSPA LA simulations, partitioned according to infiltration scenario and normalized to the regulatory limit. Expected peak doses and maximum expected doses are indicated. . . . .	4-5
4-5	Igneous scenario realizations and expected values from TSPA LA simulations, partitioned according to infiltration scenario and normalized to the regulatory limit. Expected peak doses and maximum expected doses are indicated. . . . .	4-6
4-6	Seismic scenario realizations and expected values from TSPA LA simulations, partitioned according to infiltration scenario and normalized to the regulatory limit. Expected peak doses and maximum expected doses are indicated. . . . .	4-7
4-7	Regression of maximum expected dose within a climate state to areal-average net infiltration. . . . .	4-9
4-8	Expected arrival rate normalized by source emission rate for a lognormal travel time distribution, assuming the source is constant in time once initiated but the source initiation time is uniformly distributed in time. . . . .	4-10
4-9	Expected arrival rate normalized by source emission rate for a lognormal travel time distribution, assuming the expected source is constant in time and the inventory decays in time. . . . .	4-11
4-10	Expected arrival rate normalized by source emission rate for a lognormal travel time distribution, assuming the expected source is constant in time for a fixed period. . . . .	4-12
4-11	Expected arrival rate normalized by source emission rate for a lognormal travel time distribution, assuming the expected source is constant in time for a fixed period and the inventory decays in time. . . . .	4-13
4-12	Expected release rate when releases occur at a steady rate for a finite duration $T_{src}$ and failures are spread uniformly in time between time 0 and time $T_{allf}$ . . . . .	4-16

4-13	Expected release rate when releases occur at a steady rate for a finite duration $T_{src}$ and failures are spread uniformly in time between a starting time later than time 0 and time $T_{allf}$ . . . . .	4-17
4-14	Release rate as a function of diffusion coefficients and seepage/condensation fluxes. Normalizing is relative to the case with an invert and matrix diffusion coefficient of $2 \times 10^{-9}$ m <sup>2</sup> /s without effects from volumetric water content, retardation, or tortuosity. . . . .	4-20
4-15	Cumulative seepage distribution for representative units and percolation fluxes, with seepage abstracted using trilinear interpolation. . . . .	4-22
4-16	Cumulative seepage distribution with units weighted by footprint fraction, comparing percolation flux abstractions. . . . .	4-26
4-17	Cumulative seepage distribution including uncertainty and variability. . . . .	4-27
4-18	Cumulative seepage distribution setting uncertain inputs to the median value and including variability. . . . .	4-29
4-19	Cumulative seepage distribution setting variable inputs to the median value and including uncertainty. . . . .	4-30
4-20	Cumulative seepage distribution with perfect negative correlation between $1/\alpha$ and $\log(k_f)$ . . . . .	4-31
4-21	Cumulative seepage distribution with perfect positive correlation between $1/\alpha$ and $\log(k_f)$ . . . . .	4-32
4-22	Cumulative seepage distribution, including uncertainty and variability, at the drift scale and the expected areal average. . . . .	4-34
4-23	Steady-state release for individual units with large failed area, small diffusion coefficient, no water through the waste package, and no retardation. . . . .	4-35
4-24	Steady-state release with large failed area, small diffusion coefficient, no water through the waste package, and no retardation. . . . .	4-36
4-25	Steady-state release with small failed area, small and large invert diffusion coefficient, no water through the waste package, and no retardation. . . . .	4-37

4-26 Steady-state release with small and large failed area, small diffusion coefficient, water through the waste package proportional to failed area, and no retardation.	4-39
4-27 Steady-state release with small failed area, large diffusion coefficient, no water through the waste package, comparing no invert/matrix retardation to some retardation. . . . .	4-40
4-28 Ratio of fracture to matrix release for individual units with large failed area, small diffusion coefficient, no water through the waste package, and no retardation. . .	4-41
4-29 Ratio of fracture to matrix release with large failed area, small diffusion coefficient, no water through the waste package, and no retardation. . . . .	4-42
4-30 Ratio of fracture to matrix release with small failed area, small and large diffusion coefficient, no water through the waste package, and no retardation. . . . .	4-43
4-31 Ratio of fracture to matrix release with small and large failed area, small diffusion coefficient, water through the waste package proportional to failed area, and no retardation. . . . .	4-45
4-32 Ratio of fracture to matrix release with small failed area, large diffusion coefficient, no water through the waste package, and small and large retardation. . . . .	4-46
4-33 Steady-state release with large fixed and variable failed area, small invert diffusion coefficient, no water through the waste package, and no retardation. . . . .	4-48
4-34 Steady-state release with small fixed and variable failed area, small invert diffusion coefficient, no water through the waste package, and no retardation. . . . .	4-49
4-35 Steady-state release with small fixed and variable failed area, large invert diffusion coefficient, no water through the waste package, and no retardation. . . . .	4-50
4-36 Steady-state release with small fixed and variable failed area, small invert diffusion coefficient, water through the waste package, and no retardation. . . . .	4-51
4-37 Steady-state release with large fixed and variable failed area, small invert diffusion coefficient, water through the waste package, and no retardation. . . . .	4-52
4-38 Steady-state release with small failed area, small invert diffusion coefficient, fixed and variable water through the waste package, and no retardation. . . . .	4-53



4-39 Steady-state release with large failed area, small invert diffusion coefficient, fixed and variable water through the waste package, and no retardation. . . . .	4-54
4-40 Steady-state release with small failed area, large invert diffusion coefficient, no water through the waste package, and fixed and variable retardation. . . . .	4-55
4-41 Steady-state release with small variable failed area, small invert diffusion coefficient, variable water through the waste package, and no retardation. . . . .	4-57
4-42 Transient solubility-limited release to the TLL drift shadow with 100 mm/yr dripping. . . . .	4-60
4-43 Transient solubility-limited release to the TLL drift shadow with 10 mm/yr dripping.	4-61
4-44 Transient solubility-limited release to the TLL drift shadow with 1 mm/yr dripping.	4-62
4-45 Transient solubility-limited release to the TLL drift shadow with 0.1 mm/yr dripping.	4-63
4-46 Transient dissolution-controlled release to the TLL drift shadow with 100 mm/yr dripping. . . . .	4-66
4-47 Transient dissolution-controlled release to the TLL drift shadow with 10 mm/yr dripping. . . . .	4-67
4-48 Transient dissolution-controlled release to the TLL drift shadow with 1 mm/yr dripping. . . . .	4-68
4-49 Transient dissolution-controlled release to the TLL drift shadow with 0.1 mm/yr dripping. . . . .	4-69
4-50 Transient dissolution-controlled release to the TMN drift shadow with 100 mm/yr dripping. . . . .	4-71
4-51 Transient dissolution-controlled release to the TMN drift shadow with 10 mm/yr dripping. . . . .	4-72
4-52 Transient dissolution-controlled release to the TMN drift shadow with 1 mm/yr dripping. . . . .	4-73
4-53 Transient dissolution-controlled release to the TMN drift shadow with 0.1 mm/yr dripping. . . . .	4-74

4-54	Transient solubility-limited release to the TLL drift shadow with 100 mm/yr dripping and matrix/fracture transfer. . . . .	4-75
4-55	Transient solubility-limited release to the TLL drift shadow with 10 mm/yr dripping and matrix/fracture transfer. . . . .	4-76
4-56	Transient solubility-limited release to the TLL drift shadow with 1 mm/yr dripping and matrix/fracture transfer. . . . .	4-77
4-57	Transient solubility-limited release to the TLL drift shadow with 0.1 mm/yr dripping and matrix/fracture transfer. . . . .	4-78
4-58	Transient decaying dissolution-controlled release to the TLL drift shadow with 100 mm/yr dripping. . . . .	4-79
4-59	Transient decaying dissolution-controlled release to the TLL drift shadow with 10 mm/yr dripping. . . . .	4-80
4-60	Transient decaying dissolution-controlled release to the TLL drift shadow with 1 mm/yr dripping. . . . .	4-81
4-61	Transient decaying dissolution-controlled release to the TLL drift shadow with 0.1 mm/yr dripping. . . . .	4-82
4-62	Transient solubility-limited release to the TLL drift shadow with 100 mm/yr dripping and host-rock percolation abstraction. . . . .	4-84
4-63	Transient solubility-limited release to the TLL drift shadow with 10 mm/yr dripping and host-rock percolation abstraction. . . . .	4-85
4-64	Transient solubility-limited release to the TLL drift shadow with 1 mm/yr dripping and host-rock percolation abstraction. . . . .	4-86
4-65	Transient solubility-limited release to the TLL drift shadow with 0.1 mm/yr dripping and host-rock percolation abstraction. . . . .	4-87
5-1	Voronoi polygons for the site-scale unsaturated zone flow model. Blue and red polygons represent the top and bottom of the model, respectively. Emplacement drifts are indicated in pale blue. . . . .	5-2

5-2	Upper boundary condition mean annual infiltration for the 10th, 30th, 50th, and 90th percentile maps under the present-day climate. . . . .	5-4
5-3	Upper boundary condition mean annual infiltration for the 10th, 30th, 50th, and 90th percentile maps under the monsoon climate. . . . .	5-5
5-4	Upper boundary condition mean annual infiltration for the 10th, 30th, 50th, and 90th percentile maps under the glacial-transition climate. . . . .	5-6
5-5	Upper boundary condition mean annual infiltration for the 10th, 30th, 50th, and 90th percentile maps under the post-10-ky climate. . . . .	5-7
5-6	Upper boundary condition mean annual infiltration and relative changes to percolation flux in the PTn, TSw, and as recharge for the 10th percentile maps under the present-day climate. . . . .	5-8
5-7	Upper boundary condition mean annual infiltration and relative changes to percolation flux in the PTn, TSw, and as recharge for the 30th percentile maps under the present-day climate. . . . .	5-9
5-8	Upper boundary condition mean annual infiltration and relative changes to percolation flux in the PTn, TSw, and as recharge for the 50th percentile maps under the present-day climate. . . . .	5-10
5-9	Upper boundary condition mean annual infiltration and relative changes to percolation flux in the PTn, TSw, and as recharge for the 90th percentile maps under the present-day climate. . . . .	5-11
5-10	Upper boundary condition mean annual infiltration and relative changes to percolation flux in the PTn, TSw, and as recharge for the 10th percentile maps under the monsoon climate. . . . .	5-13
5-11	Upper boundary condition mean annual infiltration and relative changes to percolation flux in the PTn, TSw, and as recharge for the 30th percentile maps under the monsoon climate. . . . .	5-14
5-12	Upper boundary condition mean annual infiltration and relative changes to percolation flux in the PTn, TSw, and as recharge for the 50th percentile maps under the monsoon climate. . . . .	5-15

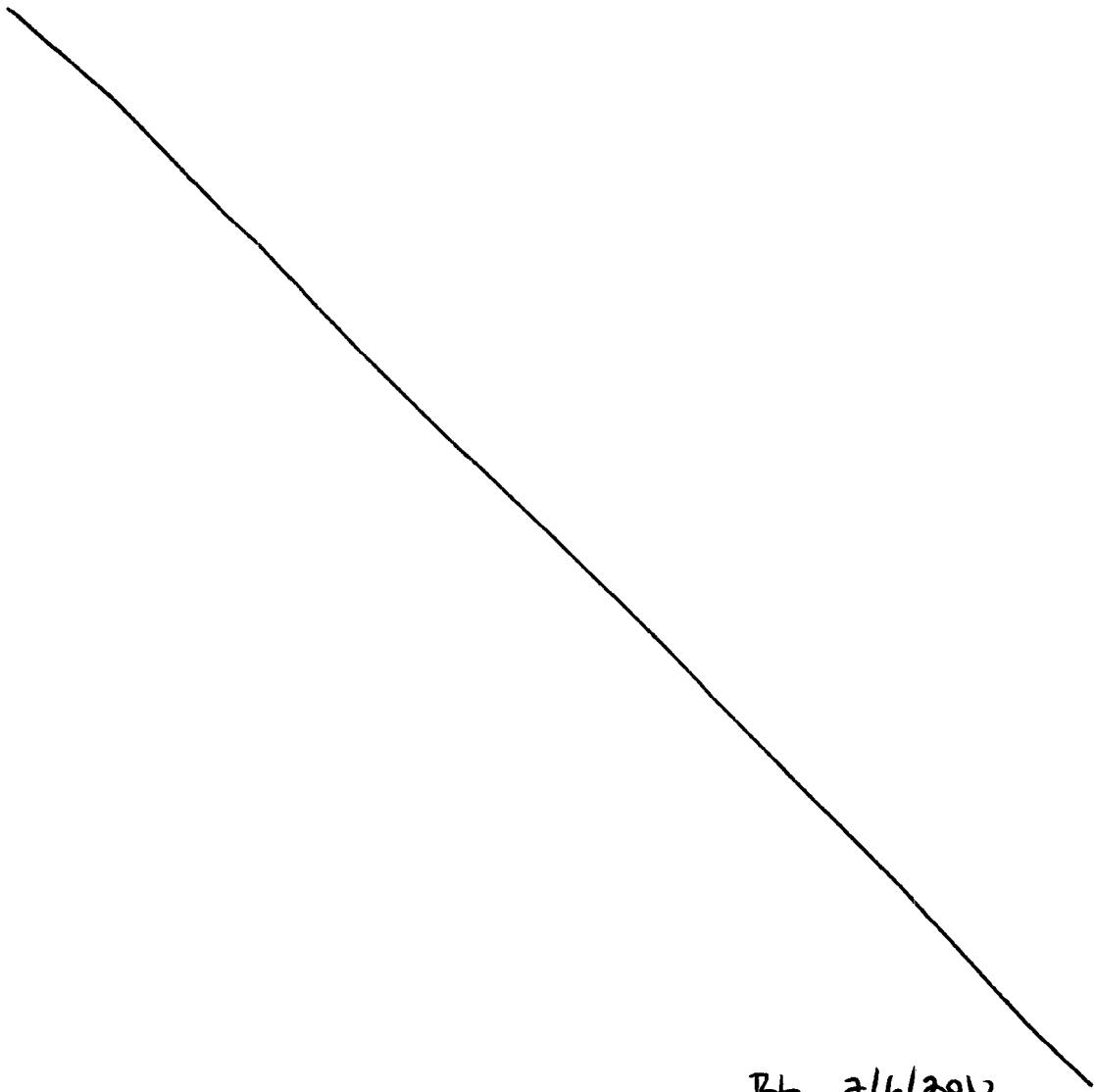
5-13 Upper boundary condition mean annual infiltration and relative changes to percolation flux in the PTn, TSw, and as recharge for the 90th percentile maps under the monsoon climate. . . . .	5-16
5-14 Upper boundary condition mean annual infiltration and relative changes to percolation flux in the PTn, TSw, and as recharge for the 10th percentile maps under the glacial-transition climate. . . . .	5-17
5-15 Upper boundary condition mean annual infiltration and relative changes to percolation flux in the PTn, TSw, and as recharge for the 30th percentile maps under the glacial-transition climate. . . . .	5-18
5-16 Upper boundary condition mean annual infiltration and relative changes to percolation flux in the PTn, TSw, and as recharge for the 50th percentile maps under the glacial-transition climate. . . . .	5-19
5-17 Upper boundary condition mean annual infiltration and relative changes to percolation flux in the PTn, TSw, and as recharge for the 90th percentile maps under the glacial-transition climate. . . . .	5-20
5-18 Upper boundary condition mean annual infiltration and relative changes to percolation flux in the PTn, TSw, and as recharge for the 10th percentile maps under the post-10-ky climate. . . . .	5-21
5-19 Upper boundary condition mean annual infiltration and relative changes to percolation flux in the PTn, TSw, and as recharge for the 30th percentile maps under the post-10-ky climate. . . . .	5-22
5-20 Upper boundary condition mean annual infiltration and relative changes to percolation flux in the PTn, TSw, and as recharge for the 50th percentile maps under the post-10-ky climate. . . . .	5-23
5-21 Upper boundary condition mean annual infiltration and relative changes to percolation flux in the PTn, TSw, and as recharge for the 90th percentile maps under the post-10-ky climate. . . . .	5-24
5-22 Southern east-west cross-section of fluxes and saturations for the 10th percentile boundary condition under the present-day climate. . . . .	5-26

5-23	South-central east-west cross-section of fluxes and saturations for the 10th percentile boundary condition under the present-day climate. . . . .	5-27
5-24	North-central east-west cross-section of fluxes and saturations for the 10th percentile boundary condition under the present-day climate. . . . .	5-28
5-25	Northern east-west cross-section of fluxes and saturations for the 10th percentile boundary condition under the present-day climate. . . . .	5-29
5-26	Western north-south cross-section of fluxes and saturations for the 10th percentile boundary condition under the present-day climate. . . . .	5-30
5-27	Central north-south cross-section of fluxes and saturations for the 10th percentile boundary condition under the present-day climate. . . . .	5-31
5-28	Eastern north-south cross-section of fluxes and saturations for the 10th percentile boundary condition under the present-day climate. . . . .	5-32
5-29	Southern east-west cross-section of fluxes and saturations for the 30th percentile boundary condition under the glacial-transition climate. . . . .	5-33
5-30	South-central east-west cross-section of fluxes and saturations for the 30th percentile boundary condition under the glacial-transition climate. . . . .	5-34
5-31	North-central east-west cross-section of fluxes and saturations for the 30th percentile boundary condition under the glacial-transition climate. . . . .	5-35
5-32	Northern east-west cross-section of fluxes and saturations for the 30th percentile boundary condition under the glacial-transition climate. . . . .	5-36
5-33	Western north-south cross-section of fluxes and saturations for the 30th percentile boundary condition under the glacial-transition climate. . . . .	5-37
5-34	Central north-south cross-section of fluxes and saturations for the 30th percentile boundary condition under the glacial-transition climate. . . . .	5-38
5-35	Eastern north-south cross-section of fluxes and saturations for the 30th percentile boundary condition under the glacial-transition climate. . . . .	5-39

List of Tables

3-1 Summary of results from sampling from distributions representing transient variation about a steady mean. Column headings are coefficient of variation. . . . . 3-2

3-2 Summary of regression coefficients and regressed MAI values given soil depth. Regression coefficients for MAI (mm/yr) and depth (m). . . . . 3-9



## 1 Aspects of infiltration

08/28/09 Analysis of precipitation duration.



This entry examines the derivation of precipitation duration used in the Mass Accounting System for Soil Infiltration and Flow (MASSIF) model (Sandia National Laboratories, 2007).

The MASSIF model uses daily time steps. Precipitation events are modeled as occurring at the start of the day, with a duration that is dependent on the daily precipitation magnitude. The event duration may be important to partitioning rainfall between local infiltration and runoff, depending on the soil characteristics. The longer duration that a particular rainfall amount occurs over, the more local infiltration is favored over runoff. However, the generalization is moot if the soil is either much more permeable or much less permeable than the range of precipitation rates for the event, because the water will all infiltrate or all run off in these cases.

The relationship between precipitation magnitude and event duration starts with a regression between the number of hours with precipitation and daily total precipitation. This regression is performed for selected climate-analog meteorological stations. The regression relationship yields (in my notation)

$$N = a + mP \quad (1-1)$$

where  $N$  is number of hours with recorded rainfall,  $P$  is total daily rainfall, and  $a$  and  $m$  are regression coefficients. The assumed event duration is then considered to be  $N - 1$ , yielding an hourly precipitation rate of

$$q = \frac{P}{a + mP - 1} \quad (1-2)$$

where  $q$  is precipitation rate.

Sandia National Laboratories (SNL) explains that the basis for the  $N - 1$  assumption is that an event of 0.5 hr is equally likely to be counted in one hour or two hours, with a mean of 1.5 hr or exactly 1 hr more than the actual duration (Sandia National Laboratories, 2007, Section 6.5.1.7). SNL further asserts that this is true for any event duration (page 6-56). To test this assumption, assume that an event of duration  $x$  can start at any time between the start and end of an hourly interval. Consider  $x = 0.25$  hr. If it starts anywhere between 0 and 0.75 hr into the interval, it counts in 1 interval, otherwise in 2. In this case, the probability that it extends over 1 interval is  $1 - x$ , and the expected  $N$  is  $0.75 \times 1 + 0.25 \times 2 = 1.25$ . Consider  $x = 0.75$  hr. The expected  $N$  is  $0.25 \times 1 + 0.75 \times 2 = 1.75$ . These tests agree with the assumption.

There are other ways of looking at the hourly data. For example, assuming that an event is recorded over  $N$  intervals, what is the probability distribution for the event duration? Consider  $N = 2$ . Here the actual event may have a duration between 0 and 2 hr. In this case, an event ending in the second hour has a uniformly distributed probability of starting at any time in the first interval. This results in a triangular probability distribution for event duration, with the peak at 1 hr and 0 probability density at 0 and 2 hr (*i.e.*, from  $N - 2$  to  $N$ ). Hourly data with longer consecutive readings (*e.g.*,  $N = 3$ ) simply offset the triangular distribution, but it always extends from  $N - 2$  to  $N$  with a peak at  $N - 1$ . Isolated hourly observations (*i.e.*,  $N = 1$ ) also have a triangular distribution with a 0 probability density at 1 ( $N$ ) and a peak at  $N - 1$ , but the distribution is asymmetric (there is no contribution from the range of  $N - 2$  to  $N - 1$ ).

Sandia National Laboratories (2007) uses a single regression to represent all events in the year, deriving regression relationships for (i) present-day climate from four on-site weather stations; (ii) upper monsoon climate from Hobbs, NM, and Nogales, AZ; (iii) lower glacial transition climate from Delta, UT; and (iv) upper glacial transition climate from Spokane, WA.

I downloaded hourly precipitation records for Spokane, Delta, Nogales, Hobbs, and Beatty from the National Climatic Data Center (NCDC). I downloaded 15-minute precipitation records for Spokane, Chewelah, Delta, and Beatty as a check. I downloaded daily precipitation records for Delta and Hobbs.

Upon inspection of the records, the hourly data for most sites and the 15-minute data at all sites is reported at increments of 0.1 in [2.54 mm]. The daily data is reported at increments of 0.01 in. The hourly data for Spokane is reported at increments of 0.01 in. Hourly data for Delta is reported at increments of 0.01 in [0.254 mm] from 1948 through September, 1980, and at 0.1 in thereafter. Hourly data for Beatty is reported at increments of 0.01 in [0.254 mm] from 1972 through March, 1978, and at 0.1 in thereafter. Hobbs data is available from several locations, each with a different interval with hourly data. The Hobbs site with COOP id 294026 is reported at hourly intervals to 0.1 mm from June, 1948, through December, 1954, and at 6-hr or 24-hr intervals from 1973 through 1999. The Hobbs 13w site (COOP id 294030) started in October, 1996, with increments of 0.1 in. Figures 6.5.1.7-1 through 6.5.1.7-4 (Sandia National Laboratories, 2007) suggest that the hourly data contained in the figures must be at a resolution finer than 0.1 in/hr, because there are instances with more than 15 consecutive hours with reported rainfall that have less than 1.5 in (38.1 mm) of total rainfall, which is the minimum amount possible to record for a 15-hr period at a rate of 0.1 in/hr.

Comparing the 15-min and 1-hr observations, it appears that the observations are accumu-



lated as time instants when a threshold volume has been achieved. For example, rain have started slowly accumulating at 0125 hr at a rate of 0.02 in/hr and continue at this rate for 6 hr. An hourly gauge recording at 0.01-in thresholds would have 0.01 in recorded at 0200, 0.02 in recorded for 0300 through 0700, and 0.01 in recorded at 0800 (seven hours with a recording). An hourly gauge recording at 0.1-in thresholds would have 0.1 in recorded at 0700 (one hour with a recording). A 15-min gauge recording at 0.1-in thresholds would have 0.1 in recorded at 0630 (one hour with a recording).

Comparing the 1-hr and daily observations, it appears that different gauges may have been used because the daily totals often do not agree even in periods with the same resolution of 0.01 in. Further, a cursory scan reveals that there are often days with rainfall recorded in one of the observation sets but not in the other. Part of this may be because the reporting time is not always at midnight, so rainfall after the reporting time may be credited to the next day, and part may be due to rounding. However, discrepancies between daily and summed hourly totals occur even with daily accumulation at midnight, and these discrepancies exceed 0.1 in for some instances (which is an awful lot to explain with rounding). It is not clear which data set is more reliable, if one is.

The digital ASCII files downloaded from the NCDC site were collected into a single spreadsheet, **Duration\_sets.xls**. I considered the year as a whole, and also broken into winter (November through February), summer (July through October), and spring (March through June). I flagged each storm according to the three seasons. I also flagged each storm according to whether the storm or an individual hour in the storm had a questionable or missing reading as flagged by NCDC. I compared the 15-min (11/12/80 through 3/1/09) and 1-hr records (7/1/48 through 9/30/80 at 0.01 in and 10/1/80 through 3/10/09 at 0.1 in resolution) for Delta. The Delta station has a reasonably long record for comparison, approximately 30 yr in each case.

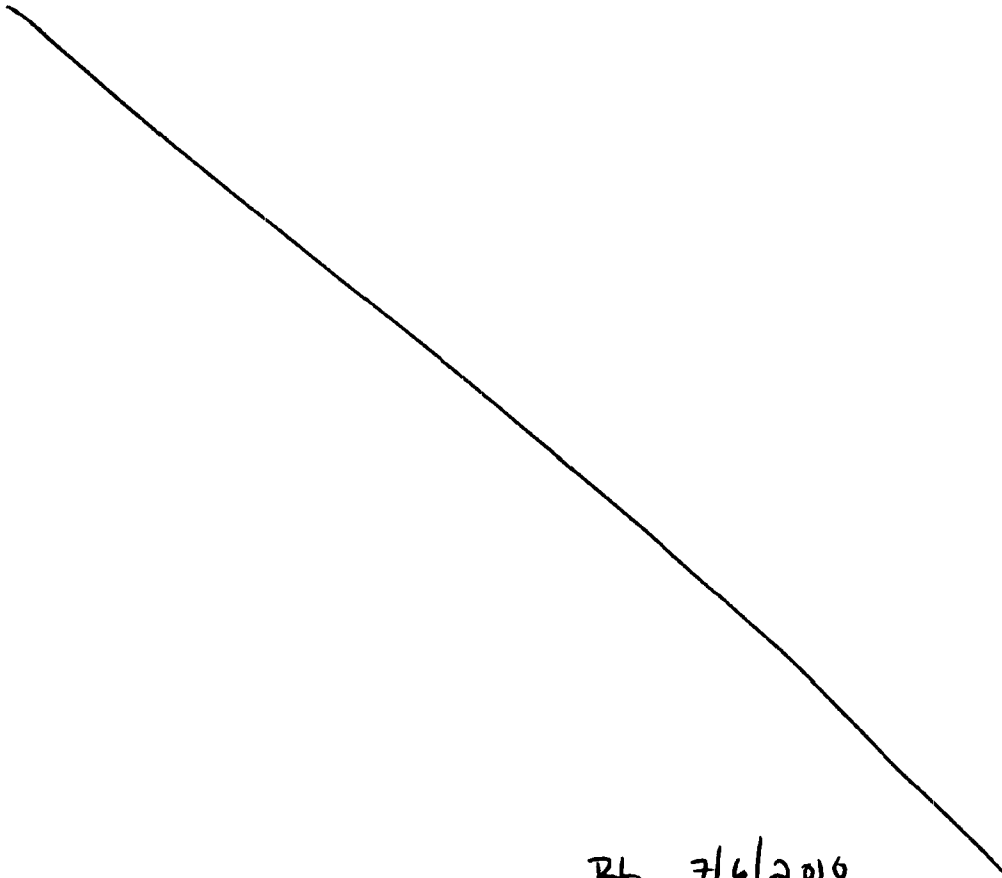
I first used the hourly Delta readings (combining the two resolutions) to estimate  $a$  and  $m$  values of 1.654 and 0.315, respectively, combining all storms. Sandia National Laboratories (2007) reports values of 1.70 and 0.34, respectively, in Table 6.5.1.7-3. The values are comparable, and the small differences are likely due to different record length and criteria for accepting storms.

Separately considering the hourly Delta data for the two resolutions, I estimate  $a$  and  $m$  values of 2.19 and 0.55 (0.01 resolution) and 0.37 and 0.27 (0.1 resolution). The fine-resolution set provides an estimate of storm duration that is approximately twice as long as the coarse-resolution set. This is probably because the fine-resolution set triggers a measurement for hours that are not triggered on the coarse-resolution set.

Broken down by season, the winter, spring, and summer values for  $m$  are 0.731, 0.544, and

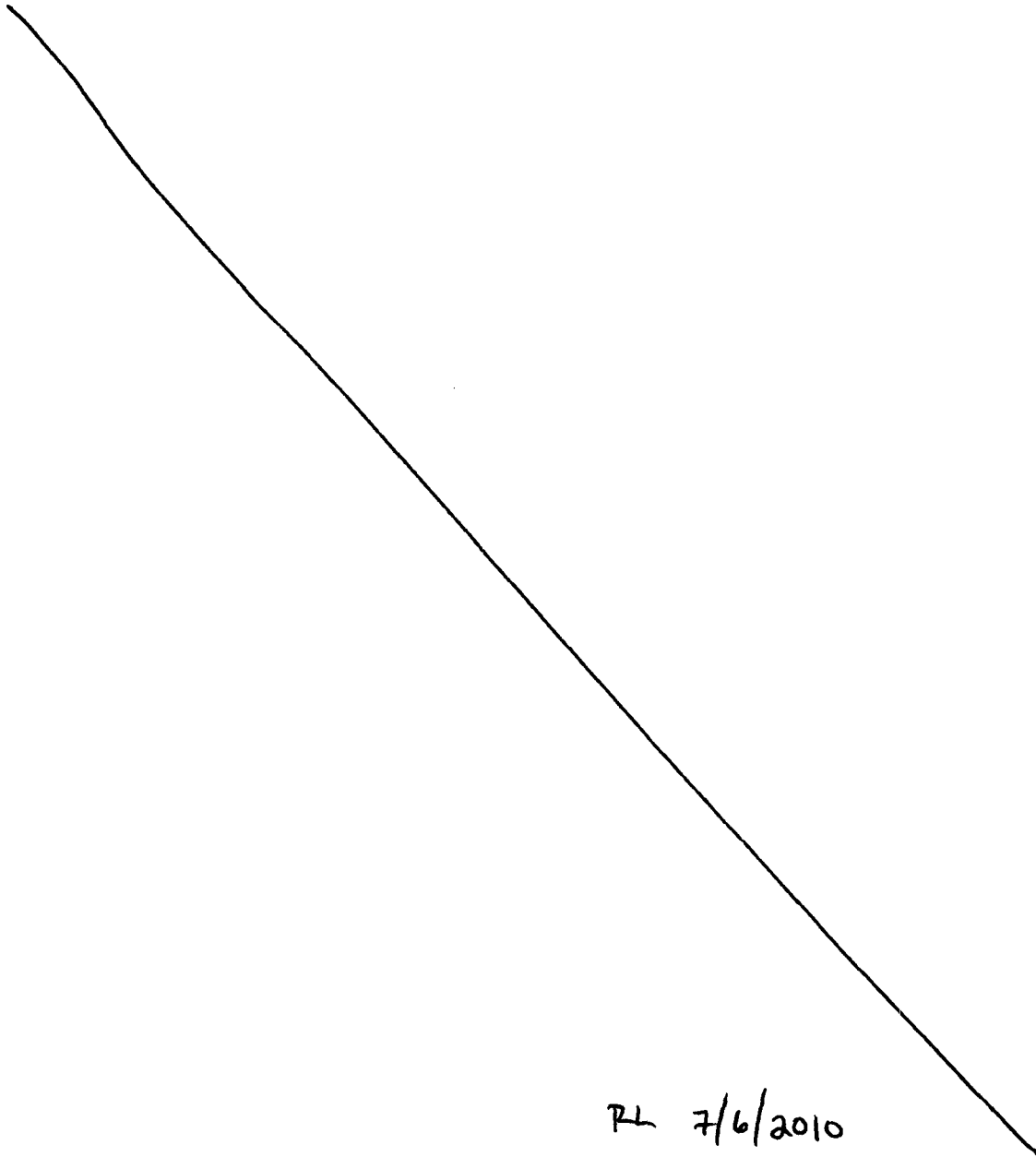
0.367 (0.01 resolution) and 0.318, 0.316, and 0.175 (0.1 resolution). Again there is a pattern with the fine-resolution storms approximately twice as long, on average, as the coarse-resolution storms. There is also a seasonal pattern where winter storms are approximately twice as long as the summer storms.

The 15-minute Delta data at the 0.1 resolution has estimated  $a$  and  $m$  values of 0.046 and 0.086, with an  $R^2 = 0.92$ . In other words, the 15-minute magnitude/duration relationship has a slope that is approximately a quarter of the 60-minute relationship with the same resolution. This is symptomatic of a measurement-triggering threshold that is coarse with respect to the duration. Winter and spring storms, considered separately, have  $R^2$  values of 0.996 and 0.977, respectively, symptomatic that these storms almost never accumulate at least 0.2 in in a single 15-minute interval. Accordingly, the 15-minute NCDC data provide little information to examine the hourly data, except perhaps for summer storms.



**References**

Sandia National Laboratories. 2007. *Simulation of Net Infiltration for Present-Day and Potential Future Climates*. ANL-NBS-HS-000032 REV 01, Department of Energy, Las Vegas, NV.



RL 7/6/2010

## 2 Infiltration, percolation, and seepage

10/26/09 Seepage and flow focusing.



This entry examines the seepage model abstraction presented by Bechtel SAIC Company, LLC (2004) with corrections presented by Bechtel SAIC Company, LLC (2007).

Bechtel SAIC Company, LLC (2004) bases the seepage model abstraction on the tabulated results from detailed process-level simulations obtained using a simulator called Seepage Model for Performance Assessment (SMPA). Each process-level SMPA simulation describes a single heterogeneous three-dimensional (3D) continuum above a drift opening, considering a spatially uniform van Genuchten  $\alpha$  parameter and a stochastically varying permeability ( $k_f$ ) parameter. The heterogeneous continuum is intended to represent small-scale variability for a fracture continuum imbedded in an impermeable matrix. In the process-level simulations, a spatially uniform background drift-scale percolation flux ( $Q_p$ ) is applied as the top boundary condition. The SMPA simulations systematically step through combinations of  $1/\alpha$ ,  $Q_p$ , and mean  $k_f$ , with 20 realizations of  $k_f$  used for each mean value of  $k_f$ . For each simulation, total seepage across the drift ceiling is calculated over a reference area corresponding to a single waste package. Bechtel SAIC Company, LLC (2004) tabulates the mean and standard deviation of the seepage flux,  $Q_s$ , from 20 realizations for a given triplet of  $1/\alpha$ , mean  $k_f$ , and  $Q_p$ . This tabulated set of values is subsequently used for performance assessment calculations.

This current analysis focuses on understanding how the model abstraction was developed from the SMPA simulations. For the purposes of understanding the abstraction, the SMPA process-level simulations are used as given. The tabulated values are provided as input files to the Total-System Performance Assessment (TSPA) as part of the License Application (LA).

TSPA uses the tabulated mean and standard deviation values obtained from the process-level simulations by sampling a value for  $1/\alpha$ , an uncertainty value for  $1/\alpha$ , a value for the mean  $k_f$  (separate values for the nonlithophysal and lithophysal units), an uncertainty value for mean  $k_f$  (again separate for the two unit types), a value for the flow focusing factor, and an uncertainty value for seepage given percolation flux. Each TSPA-sampled value represents the entire repository for each TSPA realization. Bechtel SAIC Company, LLC (2004, Section 6.7) describes the sampling procedure in detail, including parameter and uncertainty ranges.

Figure 2-1 summarizes the SMPA results and parameter abstractions used for TSPA. The horizontal axis represents  $K_f$  normalized by  $Q_p$ , consistent with Bechtel SAIC Company, LLC

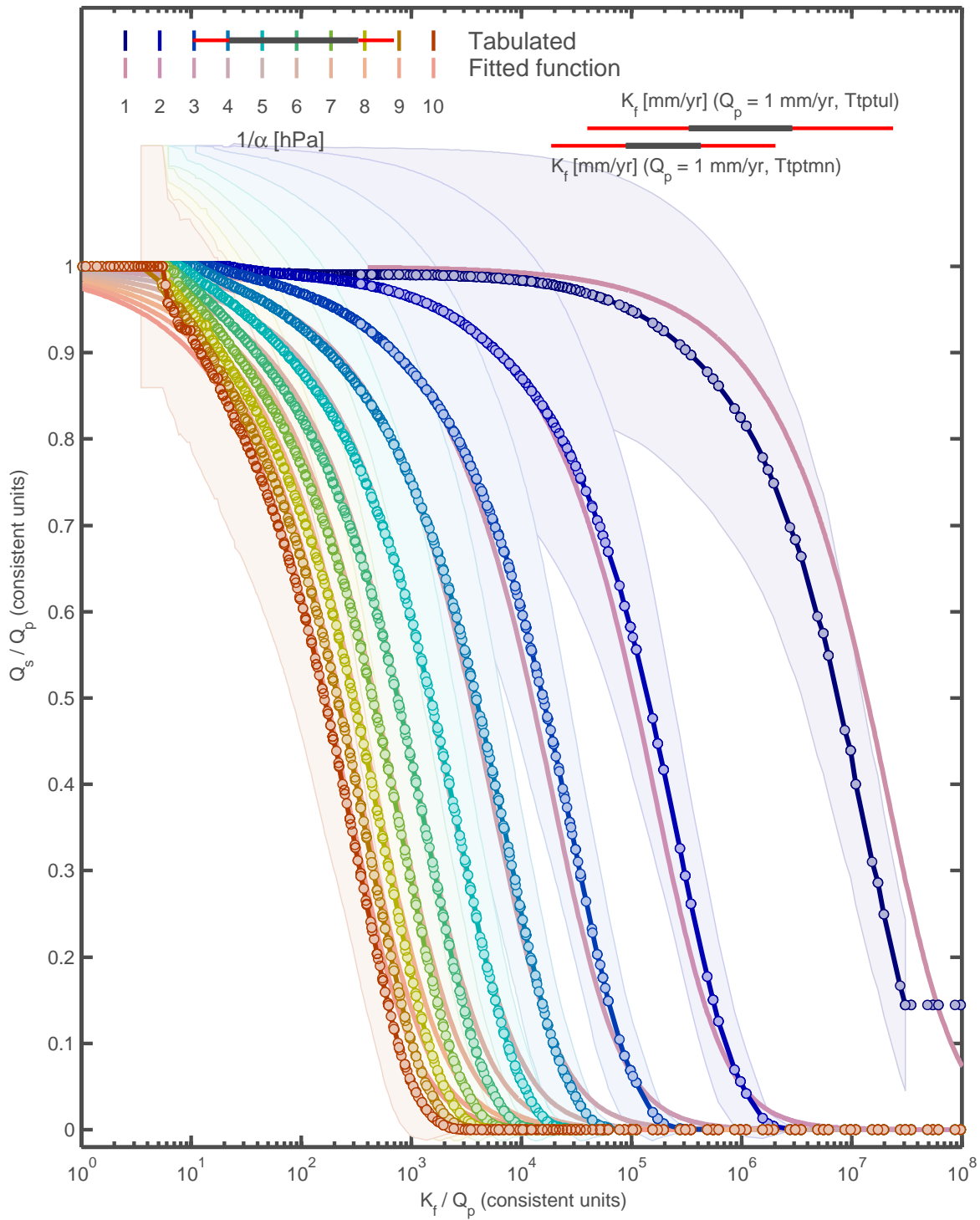


Figure 2-1: DOE abstraction for seepage in TSPA. Tabulated values indicated with circles and an independent functional form indicated by curves. Parameter values used in TSPA are indicated.

(2004, Section 6.4.2.3) describing the simulation results as uniquely depending on the ratio of  $k_f$  to  $Q_p$ . The  $K_f$  parameter represents hydraulic conductivity, which is proportional to permeability but has units of flux. The vertical axis represents seepage flux normalized by drift-scale percolation flux. The tabulated SMPA mean results are indicated as circles connected by lines in Figure 2-1, and the standard deviation for seepage flux is represented by the shaded band.

Figure 2-1 indicates the parameter abstractions used for TSPA at the top of the figure. The gray bars for  $1/\alpha$  and  $K_f$  represent the range of variability; the red bars represent the range of uncertainty superimposed on the the variability range. The TSPA abstraction adds an uncertainty to the calculated seepage results by sampling uniformly in the range of 1.7321 times the tabulated standard deviation for  $Q_s/Q_p$  above and below the mean.

Figure 2-1 also includes an independent representation of the seepage functions based on the tabulated SMPA seepage function. The independent representation uses the van Genuchten retention relationship as the fitting function. The representation in Figure 2-1 uses

$$\frac{Q_s}{Q_p} = 1 - \theta(P_c, m) \quad (2-1)$$

$$\theta(P_c, m) = \left[ 1 + |P_c|^{1/(1-m)} \right]^{-m} \quad (2-2)$$

$$P_c = \frac{P_0 F}{K_f / Q_p} \quad (2-3)$$

$$\log(1/\alpha) = a_1 \log[\log(F)] + a_2 \quad (2-4)$$

where  $1/\alpha$ ,  $K_f$ , and  $Q_p$  are the sampled values;  $m = 0.372$ ; and  $P_0 = 2.92$ . This function was determined empirically by trial and error.

The advantage of the fitted representation is that seepage values smoothly vary with the parameter values, whereas table interpolation may introduce numerical artifacts simply from the choice of interpolant. The tabulated values and independent representation are quite consistent over most of the  $Q_s/Q_p$  range, particularly for the  $1/\alpha$  values considered in TSPA. The tabulated values and independent representation differ at the  $Q_s/Q_p$  extremes, with the independent representation producing slightly less seepage at low  $k_f$  values and higher seepage at large  $k_f$  values.

Figure 2-2 compares the SMPA results with the fitted function using the TSPA parameter abstractions for parameter variability and uncertainty, and the flow focusing factor distribution, without considering seepage model uncertainty *per se*. Each of the curves in the figure represents the cumulative distribution of seepage fluxes for a given average percolation flux, with separate curves for the lithophysal (denoted Tptpul) and nonlithophysal (denoted Tptpmn) units. The star symbol in the figure represents the mean seepage for the fitted function and the diamond symbol

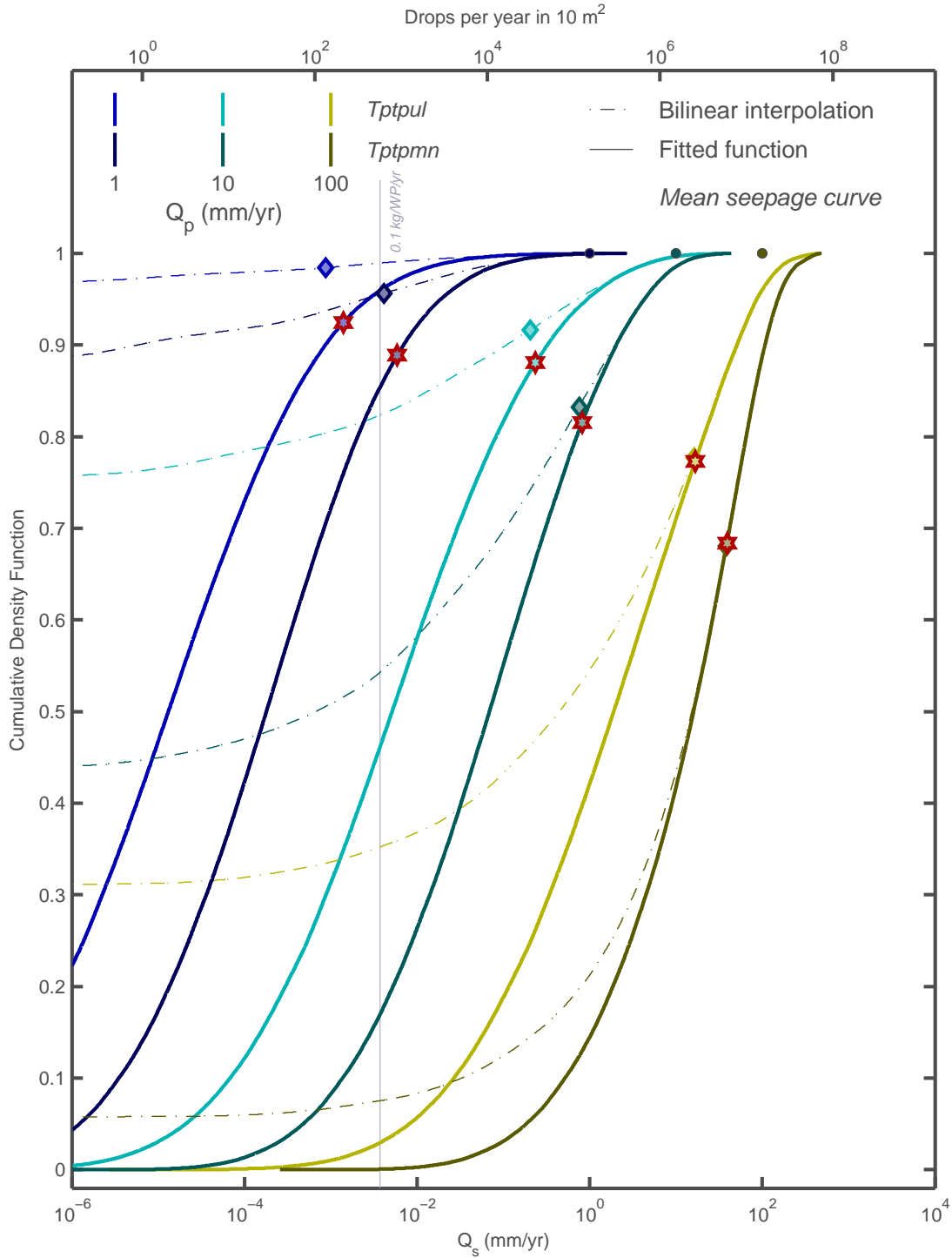


Figure 2-2: Cumulative distribution function for areal-average seepage under nominal conditions.

represents the mean seepage for the tabulated representation. The dots near the upper ends of the curves, where the cumulative density function is 1, represents the case where  $Q_s = Q_p$ . There is a small fraction of locations where  $Q_s > Q_p$  because the maximum value for the flow focusing factor is approximately 5.

In this figure, the tabulated values are interpolated using a different interpolation scheme than the trilinear interpolation described by Bechtel SAIC Company, LLC (2004, Section 6.7). The alternative interpolation scheme uses bilinear interpolation on  $1/\alpha$  and  $\log(K_f/Q_p)$ , following the suggestion by Bechtel SAIC Company, LLC (2004, Section 6.4.2.3). Interpolation is smoother with the bilinear interpolation approach, in part because there are more values of  $K_f/Q_p$  for each  $1/\alpha$  value.

Also unlike the approach described by Bechtel SAIC Company, LLC (2004, Section 6.7), seepage fluxes are not set to zero in Figure 2-2 when the seepage is below 0.1 kg/WP/yr. This seepage threshold value is indicated by the thin vertical line in Figure 2-2. The intersection of a curve with the seepage threshold value marks the fraction of locations that have seepage rates less than the threshold (*i.e.*, not seeping). As indicated by the top axis, the seepage threshold represents less than 600 drops per year on an area of 10 m<sup>2</sup>(roughly the plan area of a waste package), assuming a nominal drop diameter of 5 mm.

Each pair of curves have very similar shapes for the highest seepage fluxes, but may differ substantially for lower seepage fluxes. This difference corresponds to the different behavior for large  $K_f$  values in Figure 2-1, where the fitted function diverges from the sets of simulations. The expected values are quite similar for the two curves in each pair, because the average seepage flux is dominated by the large fluxes. Note that average percolation fluxes are between 10 and 100 mm/yr during the glacial transition and post-10,000-year climate states for all infiltration scenarios.

### 11/06/09 Seepage and flow focusing.



This entry collects the results of several sets of numerical calculations using a set of *Matlab* routines that implements the mathematical description of the drift seepage abstraction as described in the previous entry. These calculations represent confirmatory sensitivity analyses.

Figure 2-3 simply plots results that are part of TSPA calculations for the first 20 ky of performance. These results are calculated by the seepageDLL routine within TSPA. The results represent calculations for CDSP packages for the 10th percentile infiltration scenario in the glacial transition climate state. I obtained the results from Osvaldo Pensado on October 19, 2009, who



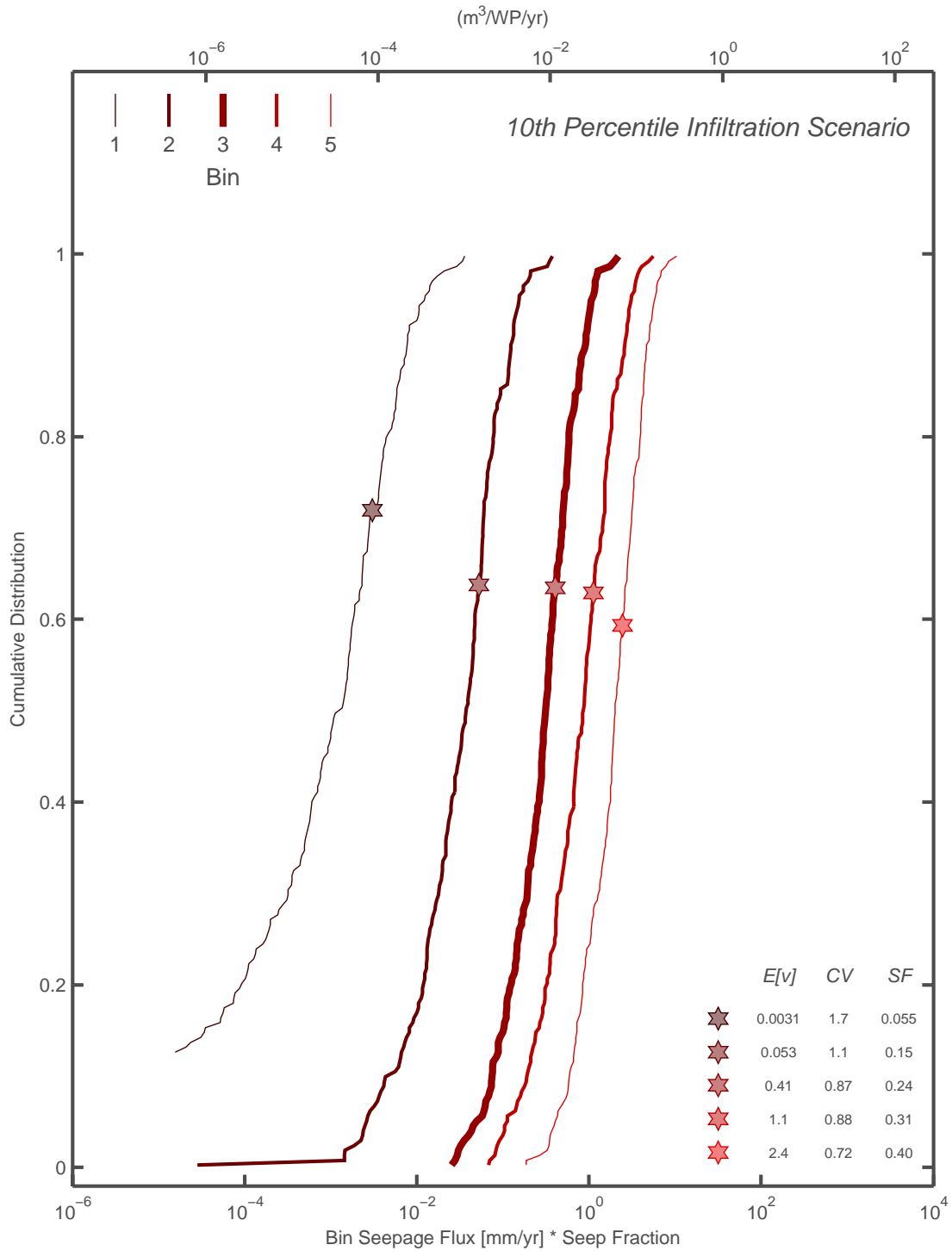


Figure 2-3: TSPA results from the seepageDLL routine for the 10th percentile infiltration scenario of the glacial transition climate for the CDSP waste packages.

extracted the results directly from the GoldSim implementation. The tabulated columns in the figure indicate (i) the mean seepage (in mm per year) for these realizations, (ii) the coefficient of variation, and (iii) the mean calculated seepage fraction for these realizations. The seepage fraction is the fraction of locations with nonzero seepage, and is tabulated as a fraction (not as a percentage, as is typical for DOE documents). Note that the bottom axis has units of mm/yr, which is directly comparable to percolation fluxes, and the top axis has units of  $\text{m}^3/\text{WP}/\text{yr}$ , which represents the total seepage flux averaged over an area of 5.1 m by 5.5 m, which is the typical format reported for seepage flux in DOE documents.

Figure 2-4 contains calculated results using the *Matlab* routines for the same climate state, variability representation, and uncertainty representation, using  $10^5$  realizations. The calculations for Figure 2-4 use bin-average percolation fluxes and consider 186 realizations of uncertainty. The TSPA calculations use percolation fluxes from the mountain-scale flow model, thus a range of percolation fluxes are found within each bin and the results in Figure 2-4 only approximately correspond to Figure 2-3. Note that there is a fairly narrow range of fluxes for most bins.

The set of dashed curves represents the cumulative distribution function for fluxes at the drift scale, and the set of solid curves represents the cumulative distribution function for the repository-average seepage. The calculations assume that 85 percent of the locations are within a nonlithophysal unit and the remaining are within a lithophysal unit, corresponding to the seepageDLL assumptions. Note that the calculated expected values and seepage fractions are essentially identical for the drift-scale and repository-average calculations, but the coefficient of variation is much smaller for the repository-average calculations. This is a result of averaging.

The minor discrepancies between expected values and seepage fractions between the drift-scale and repository-average calculations are an artifact of the calculational procedure. The drift-scale calculations use the sampled variability and uncertainty together in the calculations. For computational efficiency, the *Matlab* repository-average calculations rely on creating an intermediate table of areal-average seepage for particular sets of uncertainty parameters, then interpolates within the table with the sampled uncertainty parameters. The intermediate interpolation step introduces the minor discrepancies.

### 06/25/10 Supplemental information on seepage.



This entry collects supplemental information that I created earlier to document the model used for seepage investigations but didn't include in previous entries. The information is included for

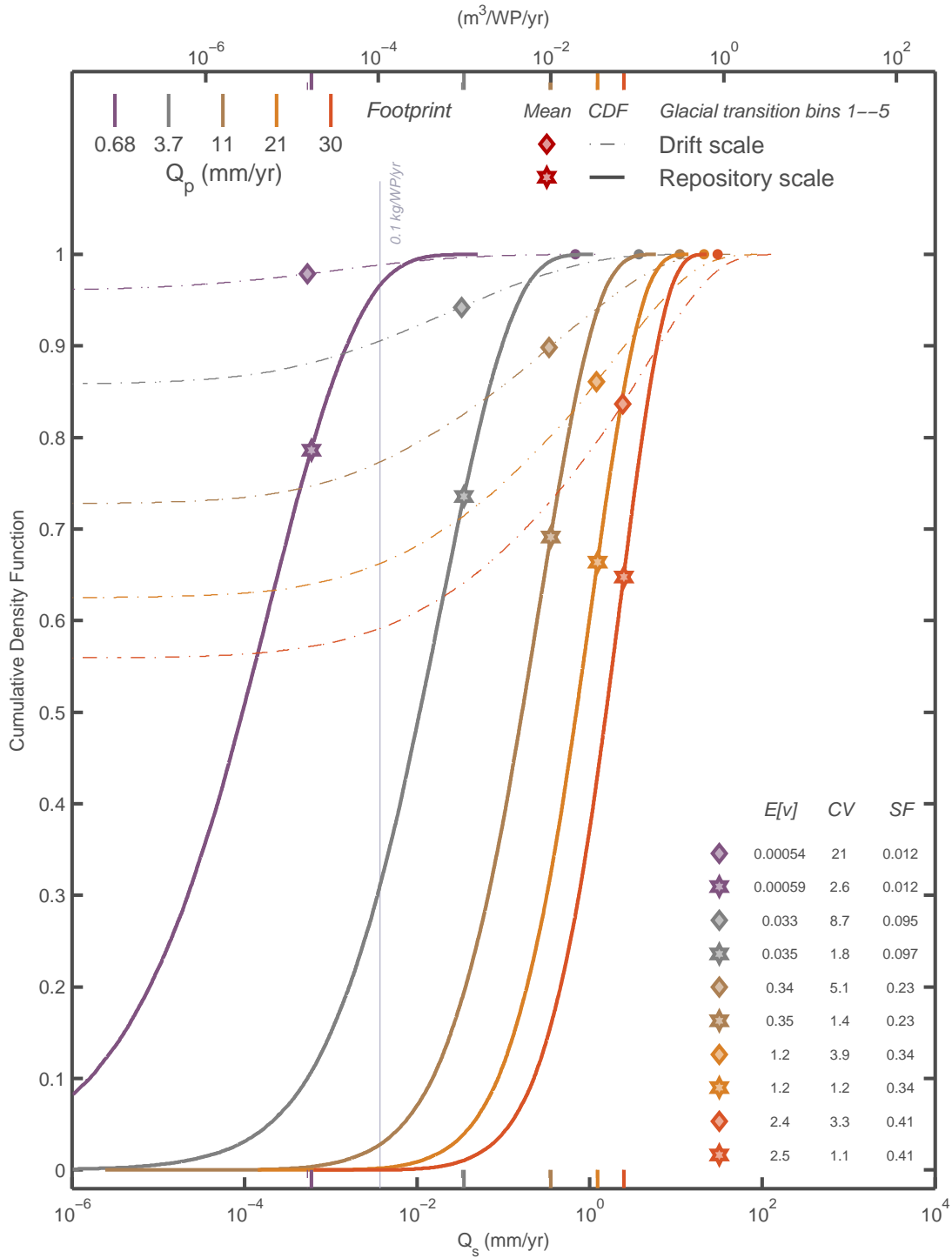
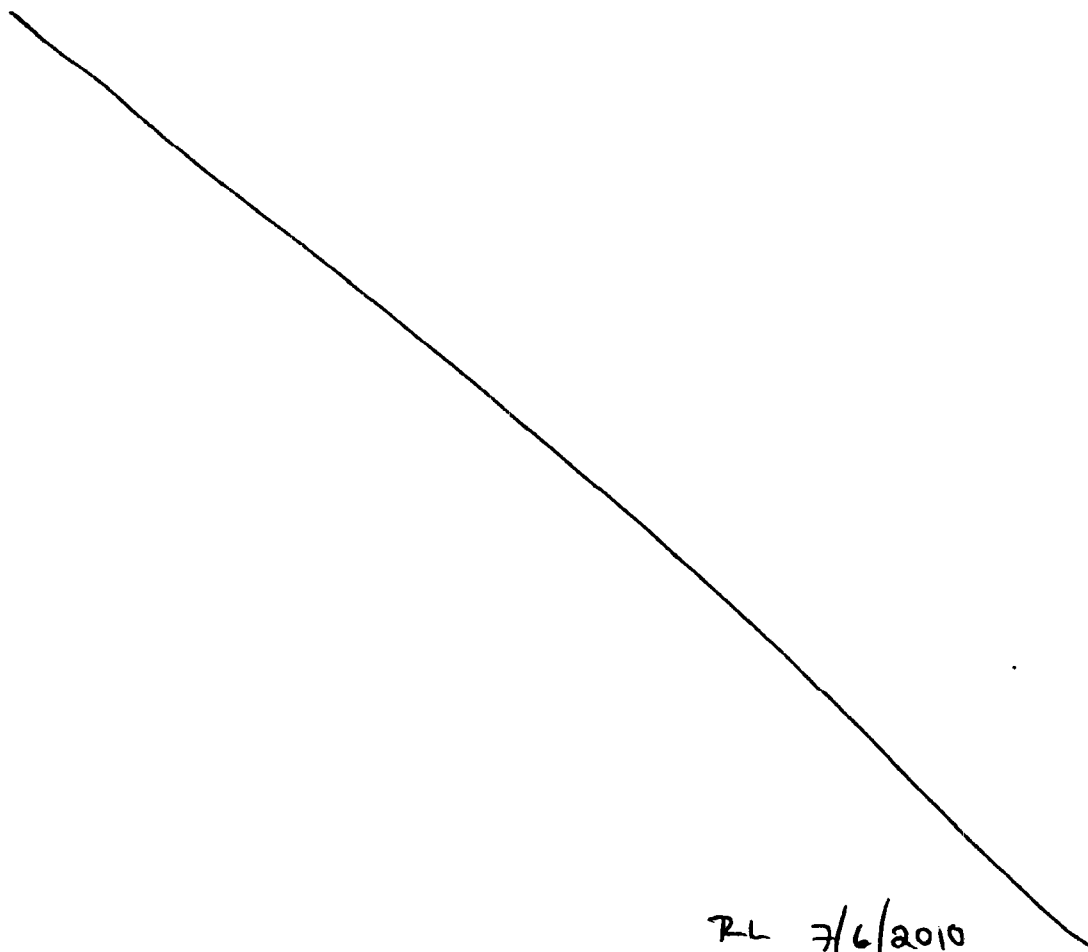


Figure 2-4: Cumulative distribution curves for the 10th percentile infiltration scenario of the glacial transition climate, comparing drift-scale and repository-average distributions.

completeness.

Section 2 describes a fitted relationship between  $1/\alpha$  and  $F = K_f/Q_p$ . Figure 2-5 compares the fitted relationship with the model results used to fit the relationship. Note that during sampling,  $1/\alpha$  generally ranges from 300 to 900 Pa when both variability and uncertainty are included and 400 to 800 Pa when just variability is included (*e.g.*, see Figure 2-1).

Lognormal distribution approximations of the nominal (DOE) flow focusing factor distribution for drift-scale percolation flux are referred to in the supplemental notes section (Section 4). Figure 2-6 compares the nominal flow focusing factor with the lognormal distributions. Each distribution has a mean value of 1, although the median value depends on the variance. The distribution with a value of  $\sigma$  has the same coefficient of variation as the nominal distribution.



RL 7/6/2010

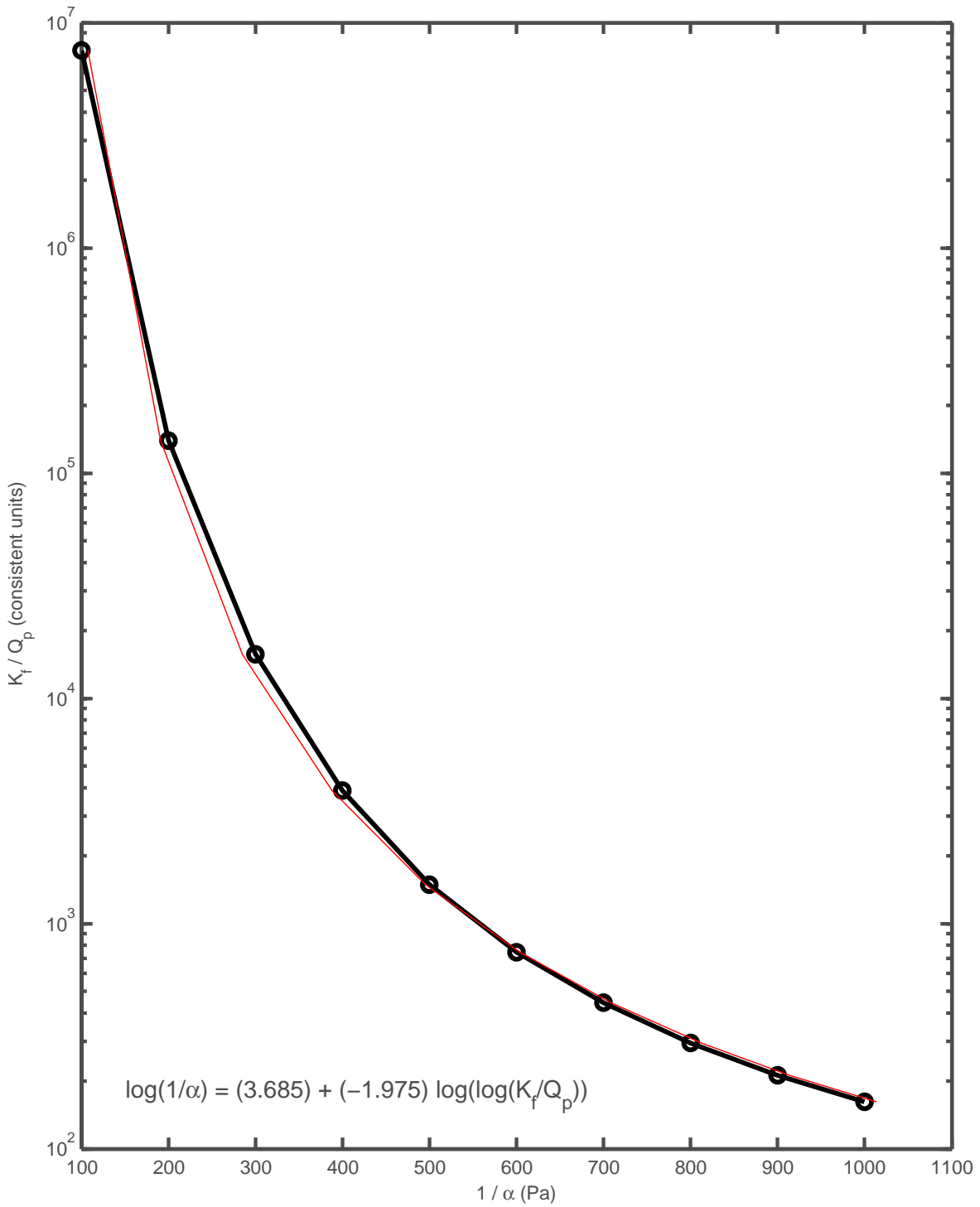


Figure 2-5: The fitted relationship (red) between  $1/\alpha$  and  $K_f/Q_p$  estimated from simulations (black).

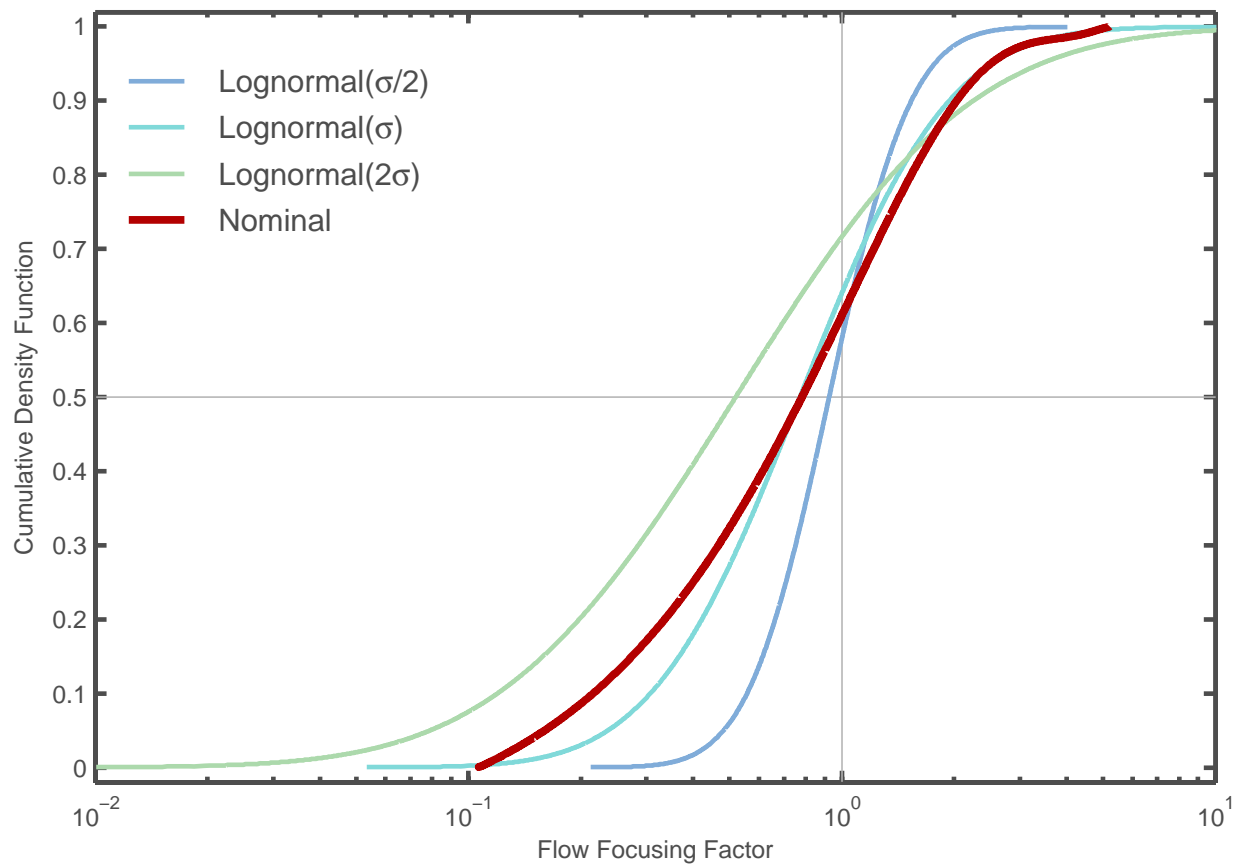
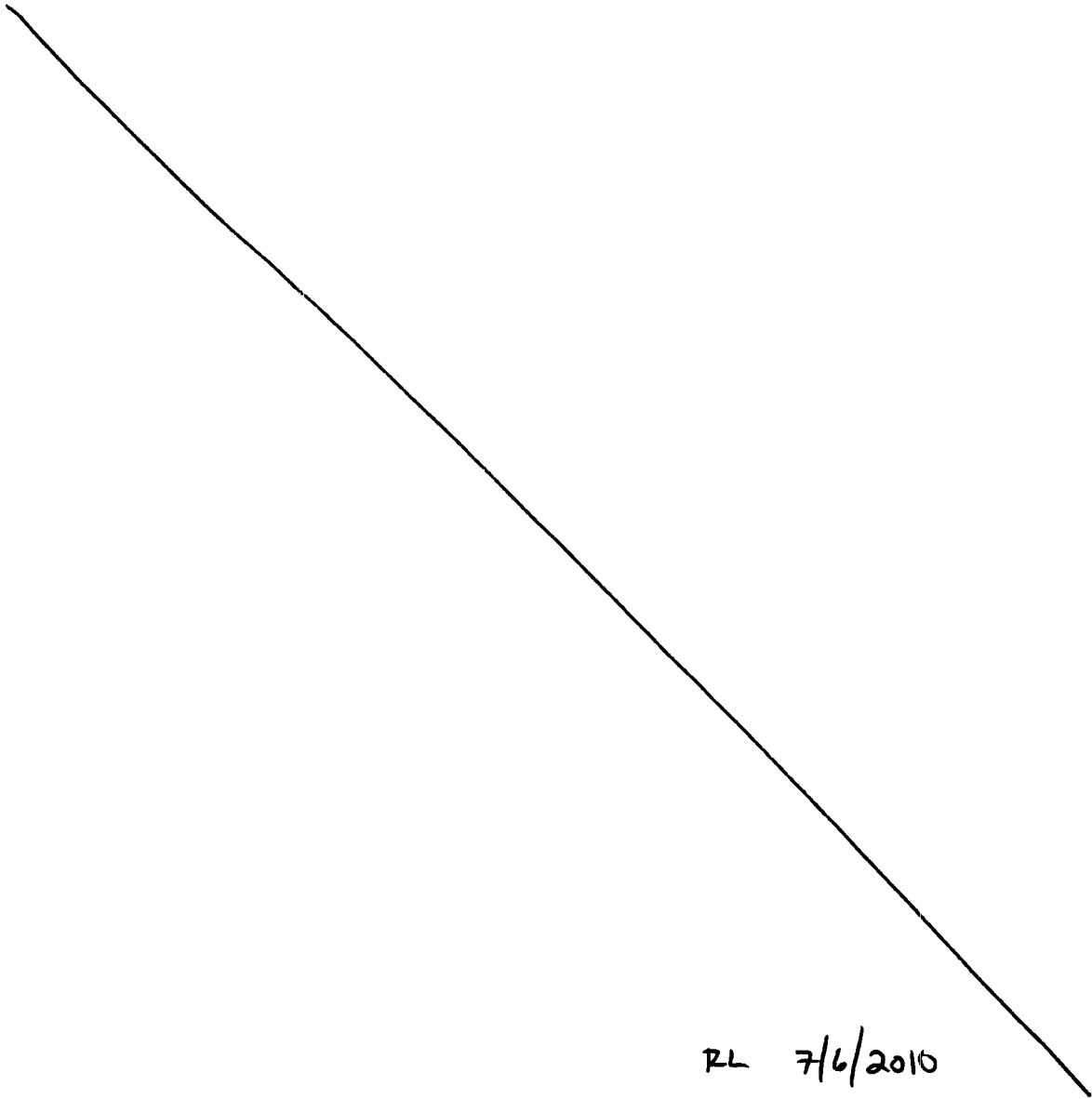


Figure 2-6: The nominal flow focusing factor representation compared with lognormal distributions having the same mean.

**References**

Bechtel SAIC Company, LLC. 2004. *Abstraction of Drift Seepage*. MDL-NBS-HS-000019 REV01, Bechtel SAIC Company, LLC, Las Vegas, NV.

Bechtel SAIC Company, LLC. 2007. *Abstraction of Drift Seepage*. MDL-NBS-HS-000019 REV01 AD01, Bechtel SAIC Company, LLC, Las Vegas, NV.



RL 7/6/2010

### 3 Safety Evaluation Review calculations

#### 04/20/10 Decadal climate variability analysis from SER Section 2.2.1.3.6.2.

This confirmatory analysis was originally documented in SER Section 2.2.1.3.6, but for the purposes of brevity is now being referenced as part of this scientific notebook. This entry records the transferred analysis with conclusions removed and explanatory information added for clarity.

The Nuclear Regulatory Commission (NRC) staff requested additional information regarding the consequences of decadal to centennial climatic fluctuations on performance assessment calculations. In response, Department of Energy (2009a, Enclosure 8) calculated a systematic increase in GLUE-weighted seepage of 2.4 and 15 percent, respectively, as a result of fluctuations in percolation flux of 20 and 50 percent about the mean (i.e., coefficients of variation of 0.2 and 0.5) under glacial transition conditions. These fluctuations are bimodally distributed as  $\pm 20$  and  $\pm 50$  of the average percolation flux. Using an analysis demonstrating that a systematic increase in GLUE-weighted seepage by a factor of approximately 2.5 has a negligible effect on the demonstration of compliance (Department of Energy, 2009c, Enclosure 5), DOE concluded by analogy that the smaller systematic increases in seepage induced by decadal to centennial climatic fluctuations also have a negligible effect on the demonstration of compliance.

I considered a more extreme range of decadal- to centennial-scale fluctuations using the DOE approach, considering bimodal, normal, and lognormal distributions for each given coefficient of variation. Climate variability representative of glacial cycles is used for a reasonable upper bound for estimating decadal- to centennial-scale infiltration fluctuations during the glacial transition climate state. I calculated seepage changes for percolation flux varying with a coefficient of variation of 0.8, roughly corresponding to mean infiltration variability over glacial cycles (Stothoff and Walter, 2007, Table 4-2), as well as 0.2 and 0.5. For comparison, Stothoff and Walter (2007, Figure 3-10) presents estimated decadal-average mean annual infiltration (MAI) over 8,000 years of the Holocene calculated from bristlecone pine tree rings; the estimated decadal-average MAI has a coefficient of variation less than 0.6. I checked an extreme value of 1.2 for good measure, which is too extreme for the bimodal and normal distributions because it creates non-physical negative percolation fluxes. The calculations were performed using a *Matlab* routine using  $10^6$  realizations, with output cut and pasted into Table 3-1. Values in parentheses are copied from Department of Energy (2009a, Enclosure 8, Tables 2 and 3). The *Matlab* routine `test_DOE_seepratecurve.m` used for the analysis is copied into the code listing appendix for this project.

The resulting GLUE-weighted systematic increase in average seepage is approximately 40 per-



Table 3-1: Summary of results from sampling from distributions representing transient variation about a steady mean. Column headings are coefficient of variation.

Scenario	MAI (mm/yr)	Transient seepage divided by steady seepage			
		0.2 (RAI Table 2)	0.5 (RAI Table 3)	0.8	1.2
Bimodal					
10th	12.2	1.029 (1.029)	1.182 (1.182)	1.474	--
30th	26.3	1.026 (1.026)	1.162 (1.162)	1.421	--
50th	36.2	1.025 (1.024)	1.153 (1.153)	1.400	--
90th	69.7	1.021 (1.021)	1.133 (1.133)	1.348	--
GLUE	57.7	1.024 (1.024)	1.152 (1.152)	1.398	--
Normal					
10th	12.2	1.029	1.185	1.457	--
30th	26.3	1.026	1.164	1.408	--
50th	36.2	1.025	1.156	1.389	--
90th	69.7	1.021	1.136	1.341	--
GLUE	57.7	1.024	1.155	1.387	--
Lognormal					
10th	12.2	1.029	1.172	1.406	1.806
30th	26.3	1.025	1.150	1.348	1.665
50th	36.2	1.024	1.141	1.322	1.607
90th	69.7	1.021	1.118	1.263	1.482
GLUE	57.7	1.024	1.140	1.320	1.606

cent of the steady seepage under glacial transition conditions for the glacial-cycle variability (coefficient of variation equals 0.8). The bimodal, lognormal, and normal distributions give similar results. Systematically increasing GLUE-weighted seepage by a factor of 2.5 using the lognormal distribution requires approximately 2.5 for a coefficient of variation, far more extreme than glacial variability.

#### 04/21/10 Episodic flow analysis from SER Section 2.2.1.3.6.2.



This confirmatory analysis was originally documented in SER Section 2.2.1.3.6, but for the purposes of brevity is now being referenced as part of this scientific notebook. This entry records the

transferred analysis with conclusions removed and explanatory information added for clarity.

I considered the consequences of episodic flow using information provided by the applicant in an RAI response (Department of Energy, 2009c, Enclosure 3, Tables 4 and 5). For a bounding calculation, I assumed that episodic flow completely avoids the capillary barrier and becomes seepage. This bounding assumption represents an extreme breach of the DOE model, in which more than 92 percent of percolating flux is diverted even in the highest flux locations (*i.e.*, Percolation Bin 5 during the post 10,000 year climate state). The calculation does not pertain to the igneous intrusion case after disruption, because DOE assumes that no capillary diversion occurs once the intrusion event occurs. To perform the bounding calculation, I used a weighted average of bin-average seepage calculated by (Department of Energy, 2009c, Enclosure 3, Table 5) and the corresponding average percolation fluxes for the same bins calculated by Department of Energy (2009c, Enclosure 3, Table 4), for the climate states after the thermal pulse ends (the monsoon, glacial-transition, and post-10,000-year climate states).

My calculation is documented in worksheet **EpisodicFlowCalc** of spreadsheet **SERSeep-Calcs.xls**. I combined the two provided tables then added differing assumptions regarding seepage efficiencies.

I first calculated the consequence based on the DOE estimate that one percent of the repository area is affected by fast pathways under episodic flows. I calculated the seepage and seepage fraction for percolation flux bin  $i$  using

$$q_{si1} = (1 - f)q_{si0} + fq_{pi}\epsilon \quad (3-1)$$

$$F_{si1} = (1 - f)F_{si0} + f \quad (3-2)$$

where  $q_{si0}$  and  $q_{si1}$  are original and new seepage fluxes for bin  $i$ ,  $F_{si0}$  and  $F_{si1}$  are original and new seepage fractions for bin  $i$ ,  $q_{pi}$  is bin-average percolation flux (same units as  $q_{si}$ ),  $f$  is the fraction of the bin affected by the fast pathways, and  $\epsilon$  is the seepage efficiency. Total seepage is calculated by summing the percolation flux bins

$$q_s = \sum_{i=1}^N w_i q_{si} \quad (3-3)$$

$$Q_s = \sum_{i=1}^N w_i q_{si} F_{si} \quad (3-4)$$

$$F_s = \sum_{i=1}^N w_i F_{si} \quad (3-5)$$

where  $q_s$  is the seepage rate for seeping areas,  $Q_s$  is the repository-average seepage rate (seeping

plus nonseeping),  $F_s$  is the repository-average seepage fraction, and  $w_i$  is the area fraction for each bin. The  $Q_s$  parameter is most relevant for comparisons because it represents total seeping flux. Columns BB through BI in EpisodicFlowCalc contain this general calculation specifying  $f$  and  $\epsilon$  for each bin. Other columns document specific assumptions. The Clean worksheet summarizes the calculations, cut and pasted from worksheet EpisodicFlowCalc and formatted for clarity.

If episodic flow is equally likely to affect the repository regardless of percolation flux and 1 percent of the repository is affected,  $f = 0.01$  and  $\epsilon = 1$  for all bins. For this case the bounding areal-average seepage rate  $Q_s$  is 1.18 to 1.19 times larger than the DOE-calculated (steady) seepage rate for the post-thermal-pulse climate states.

The largest relative increase occurs in Bin 1. Assuming that Bin 1 experiences perfectly efficient episodic flow and the remaining areas are steady (5 percent of the repository area experiences perfectly efficient seepage in the low-flow areas),  $f = 1$  and  $\epsilon = 1$  in Bin 1 and  $f = 0$  elsewhere. These assumptions result in between 100 and 250 times larger seepage fluxes in Bin 1. Repository-average seepage flux only increases between 1.07 and 1.14 times because the available percolation flux is small in Bin 1.

The smallest relative increase but largest absolute increase occurs in Bin 5. When episodic flow is assumed to be strongly associated with large percolation fluxes (i.e., only Percolation Bin 5 is weighted), assuming that one percent of flows are strongly episodic ( $f = 0.2$  and  $\epsilon = 1$  in Bin 5 and  $f = 0$  elsewhere) yields  $Q_s$  that is 1.28 to 1.39 times larger than the DOE-calculated seepage rate.

As an extreme bounding case, I calculated the consequence of a complete breach in the barrier capability for the areas with fast pathways, assuming that the area experiencing fast pathways is five times larger than the DOE estimate and assuming that the fast pathways correspond to the highest fluxes. Associating episodic flows with Bin 5 ( $f = 1$  and  $\epsilon = 1$  in Bin 5 and  $f = 0$  elsewhere),  $Q_s$  increases by a multiple of 2.4 to 2.9. For comparison,  $Q_s$  increases by a multiple of 3.9 (long-term-average) to 7.1 (monsoon) relative to the GLUE-weighted DOE steady-state value, and  $F_s$  increases by a factor of 1.06 (i.e., 6 percent larger), under the same assumptions for  $f$  and  $\epsilon$  if the original MASSIF-calculated weights are used instead of the GLUE weights.

For comparison, (Department of Energy, 2009c, Enclosure 1) considered the dose consequences of spatial focusing for the million-year seismic ground motion case. For the most extreme case considered (Case 6c),  $Q_s$  increased by 3.9 and  $F_s$  decreased by 32 percent.

**04/22/10 Temporal variability from SER Section 2.2.1.3.5.3.2.2.**

This confirmatory analysis was originally documented in SER Section 2.2.1.3.5, but for the purposes of brevity is now being referenced as part of this scientific notebook. This entry records the transferred analysis with conclusions removed and explanatory information added for clarity.

I compared DOE's mathematical representation of precipitation (Sandia National Laboratories, 2007, Appendix F) with summary observations from meteorological stations DOE used to represent mean winter and summer precipitation for potential future climate states. I used 10,000 realizations of a 1,000-year precipitation sequence for each of the present day, monsoon, and glacial transition climate states, with each realization obtained by sampling from the parameters listed in Sandia National Laboratories (2007, Tables F-22 through F-24), to evaluate the statistical properties of DOE's precipitation representation. I considered annual, cold weather (November through March), and hot weather (June through September) precipitation.

The sampled sequences are displayed in Figure 3-1 (present-day climate), Figure 3-2 (monsoon climate), and Figure 3-3 (glacial-transition climate). Monthly summaries are plotted in the top subfigure, the cumulative distribution of seasonal and annual precipitation in the middle subfigure, and a scatterplot between seasonal and annual precipitation in the bottom subfigure. The yellow scatterplot points represent a winter/summer comparison rather than a seasonal/annual comparison. The sampling and plotting are performed using *Matlab* routines in **test\_massif\_precip.m**.

The statistical model mean annual precipitation (MAP) agreed with observations to within 10 percent for all 3 climate states, and the statistical model provided a wider range of extreme values than observed for all seasons in all 3 climate states. The statistical-model mean cold weather precipitation agreed with observations to within 16 percent for all 3 climate states. There is uncertainty in estimating MAP from observations. For example, average precipitation totals from 1994 through 2006 for five Yucca Mountain Project meteorological stations, reported in SAR Tables 1.1-10 through 1.1-12, 1.1-15, and 1.1-18, differ on average by approximately 7 percent from values for 1993 through 2004 reported in Sandia National Laboratories (2006, Table 6.1-4).

**04/22/10 Uncertain soil depth from SER Section 2.2.1.3.5.3.3.**

This confirmatory analysis was originally documented in SER Section 2.2.1.3.5.3.3, but for the purposes of brevity is now being referenced as part of this scientific notebook. This entry records the transferred analysis with conclusions removed and explanatory information added for clarity.

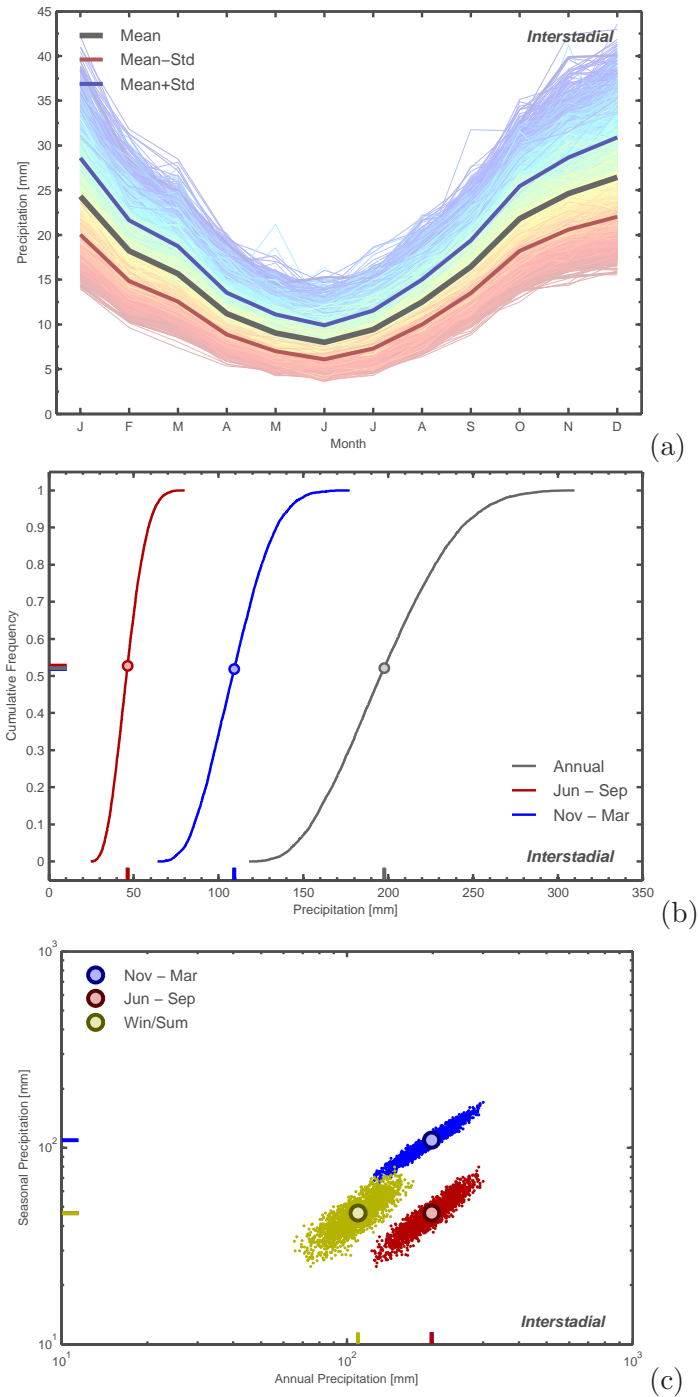


Figure 3-1: Simulated precipitation sequences using SNL parameters for present-day climate and 10,000 realizations. (a) Monthly precipitation sequences, (b) cumulative frequency, and (c) correlation between annual and seasonal precipitation.

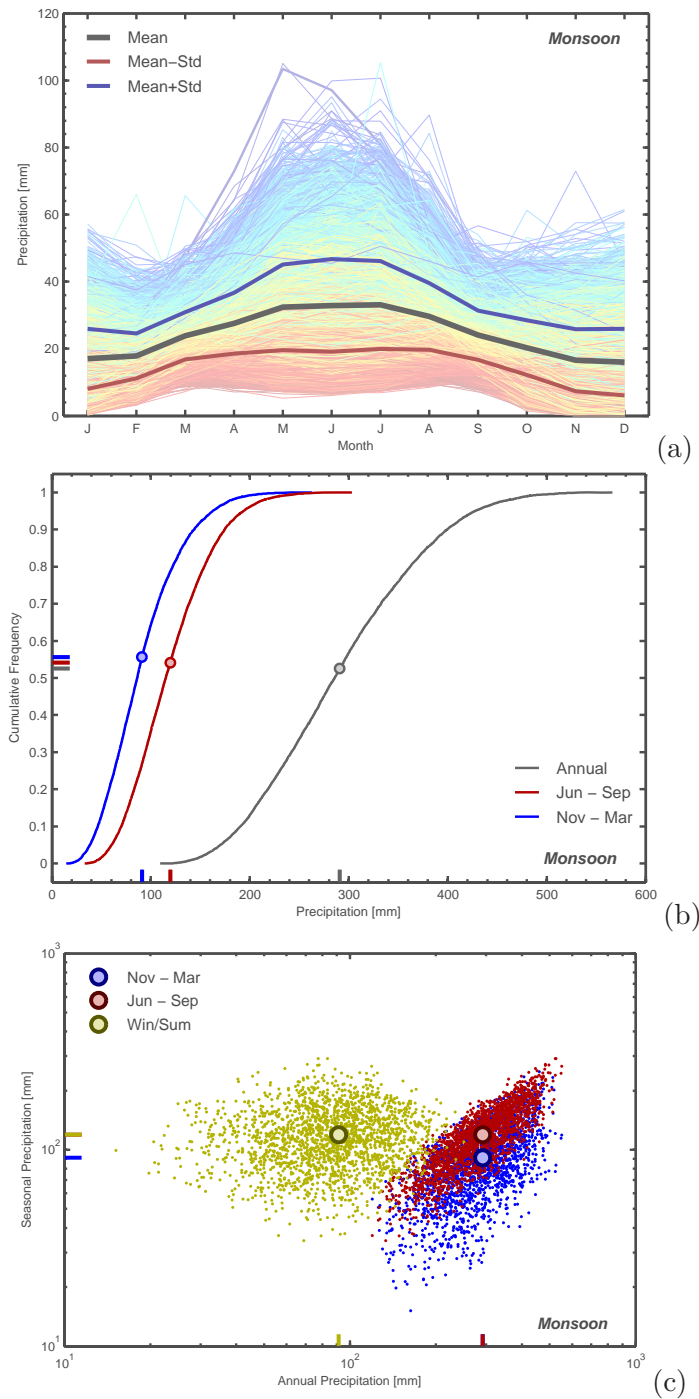


Figure 3-2: Simulated precipitation sequences using SNL parameters for monsoon climate and 10,000 realizations. (a) Monthly precipitation sequences, (b) cumulative frequency, and (c) correlation between annual and seasonal precipitation.

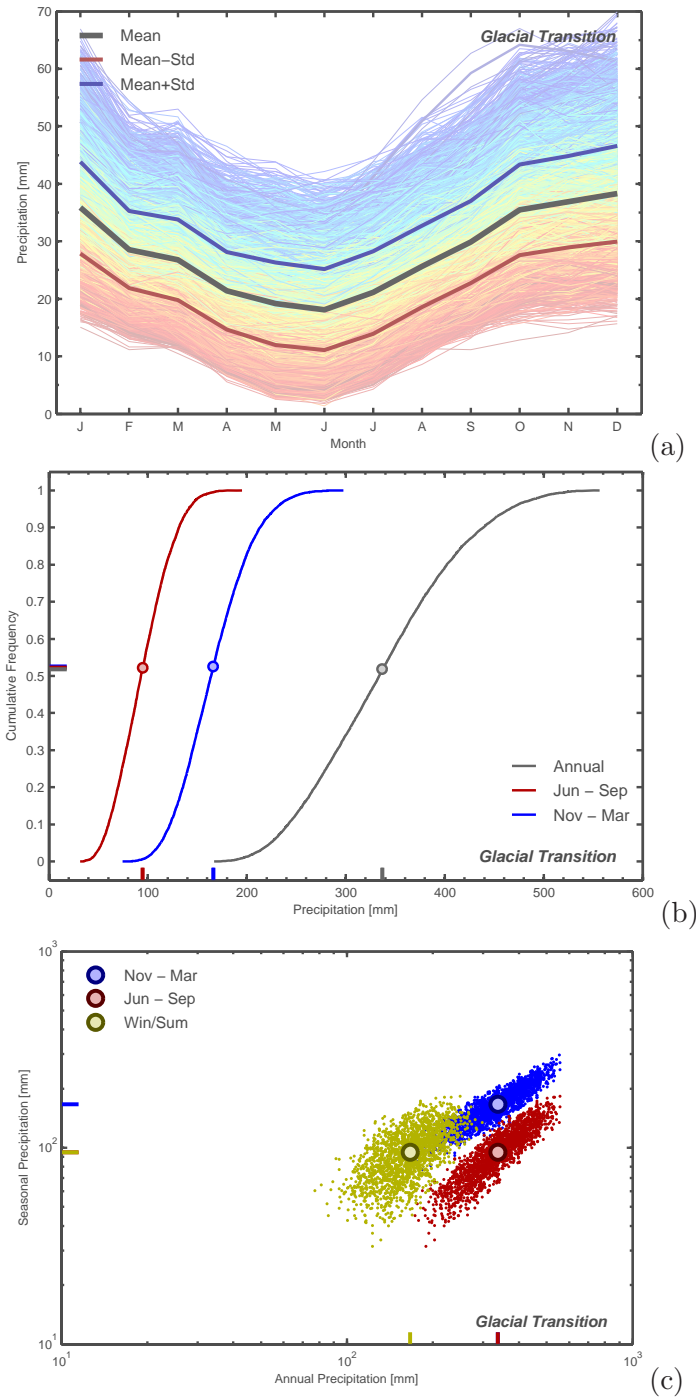


Figure 3-3: Simulated precipitation sequences using SNL parameters for glacial-transition climate and 10,000 realizations. (a) Monthly precipitation sequences, (b) cumulative frequency, and (c) correlation between annual and seasonal precipitation.

Table 3-2: Summary of regression coefficients and regressed MAI values given soil depth. Regression coefficients for MAI (mm/yr) and depth (m).

Regression	<i>b</i>	<i>a</i>	MAI (mm/yr) given soil depth (m)				MAI ratio	
			0.10	0.50	0.20	0.30	0.1/0.5	0.2/0.3
Linear present	-45.42	24.30	19.76	1.59	15.2	10.7	12.45	1.43
Exponential present	-12.98	-6.07	23.82	2.93	14.8	9.6	8.13	1.55
Power-law present	-1.17	0.66	28.88	4.37	12.8	8.0	6.61	1.61
Linear glacial	-87.33	56.38	47.65	12.71	38.9	30.2	3.75	1.29
Exponential glacial	-24.11	-0.91	54.59	15.80	37.9	28.1	3.46	1.35
Power-law glacial	-0.79	2.31	62.13	17.39	35.9	26.0	3.57	1.38

The statistical distribution that DOE uses to describe effective soil depth in Soil Depth Class 4 may systematically affect MAI estimates. The uniform distribution has a median value of 0.3 m, compared to the median values of soil depth of approximately 0.25 m in the DOE- and NRC-observed soil depths (Sandia National Laboratories, 2007, Table 6.5.2.4-2[a] and Section 7.2.4[a]) and in the DOE-calculated cumulative distribution function for estimates of mean soil depth (Department of Energy, 2009b, Enclosure 5, Figure 2).

I used the applicants sensitivity analyses for fixed aleatory uncertainty under present-day and glacial-transition climate states (Sandia National Laboratories, 2007, Figures H-3, H-4, H-11, and H-12) to estimate the consequence of decreasing median soil depth. I digitized the figures to get MAI and soil depth pairs. These are collected and sorted in worksheet **Summary of the Soil\_vs\_MAI\_Digitized.xls** spreadsheet. I regressed the calculated net infiltration results in these figures against the corresponding effective soil depth. I tried linear, logarithmic, and power-law representations with similar values for  $R^2$  (0.71 for glacial-transition, 0.59 to 0.65 for present-day).

The linear regression has the form

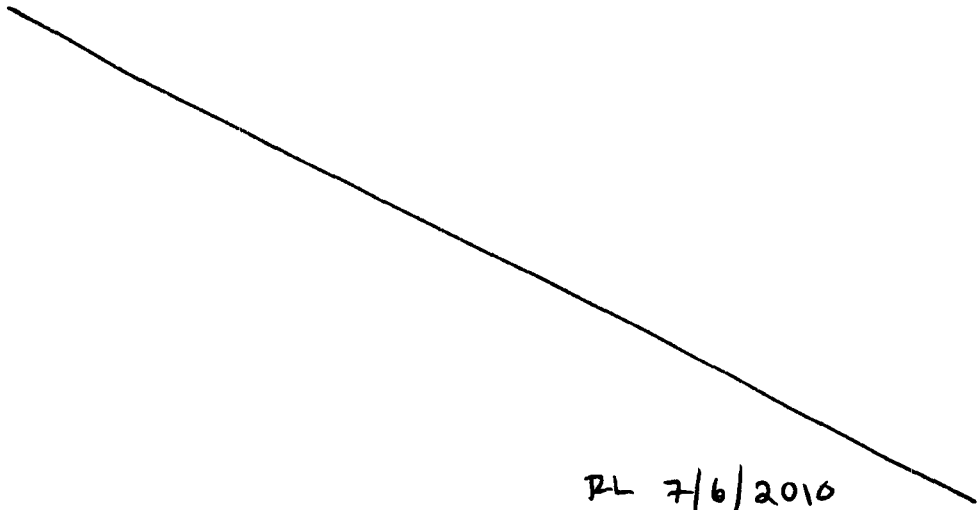
$$I = a + bD \quad (3-6)$$

where  $I$  is MAI [mm/yr],  $D$  is soil depth [m], and  $a$  and  $b$  are fitting constants. With these units,  $a = 19.76$  and  $b = -45.42$  for the present-day climate and  $a = 56.38$  and  $b = -87.33$  for the glacial-transition climate. The full set of regressed coefficients, MAI values for representative soil depths, and differences in MAI with respect to soil depth are shown in Table 3-2.



## References

- Department of Energy. 2009a. Yucca Mountain–Response to Request for Additional Information Regarding License Application (Safety Analysis Report Section 2.2), Safety Evaluation Report Volume 3, Chapter 2.2.1.2.1, Set 5. Letter (June 5) J.R. Williams to J.H. Sulima (NRC).
- Department of Energy. 2009b. Yucca Mountain–Response to Request for Additional Information Regarding License Application (Safety Analysis Report Section 2.3.1), Safety Evaluation Report Volume 3, Chapter 2.2.1.3.5, Set 1. Letter (June 24) J.R. Williams to J.H. Sulima (NRC).
- Department of Energy. 2009c. Yucca Mountain–Response to Request for Additional Information Regarding License Application (Safety Analysis Report Sections 2.3.2 and 2.3.3), Safety Evaluation Report Volume 3, Chapter 2.2.1.3.6, Set 1. Letter (June 1) J.R. Williams to J.H. Sulima (NRC).
- Sandia National Laboratories. 2006. *Data Analysis for Infiltration Modeling: Extracted Weather Station Data Used to Represent Present-Day and Potential Future Climate Conditions in the Vicinity of Yucca Mountain*. ANL-MG-MD-000015 REV 00, Sandia National Laboratories, Las Vegas, NV.
- Sandia National Laboratories. 2007. *Simulation of Net Infiltration for Present-Day and Potential Future Climates*. ANL-NBS-HS-000032 REV 01, Department of Energy, Las Vegas, NV.
- Stothoff, S. and G. Walter. 2007. *Long-Term-Average Infiltration at Yucca Mountain, Nevada: Million-Year Estimates*. CNWRA 07-003, Center for Nuclear Waste Regulatory Analyses, San Antonio, TX.



RL 7/6/2010